# NUMERICAL INVESTIGATION OF AN INFLATABLE

# AERODYNAMIC BOATTAIL FOR TRACTOR-TRAILERS

by

KANTHASAMY ELANKUMARAN, B.S.E.

A THESIS

IN

MECHANICAL ENGINEERING

Submitted to the Graduate Faculty
of Texas Tech University in
Partial Fulfillment of
the Requirements for
the Degree of

MASTER OF SCIENCE

IN

MECHANICAL ENGINEERING

Approved

May, 1997

# ACKNOWLEDGMENTS

First of all, I would like to express my gratitude and thanks to my graduate advisor Dr. S. Parameswaran for introducing me to the fascinating world of computational fluid dynamics and guiding me to produce this thesis.

I would also like to extend my thanks to the thesis committee members Dr. J.W. Oler and Dr. T.T. Maxwell for their invaluable suggestions and time.

My special thanks are due to Mr. Sadek Rahman for helping me to learn the inside out of the software available in the CFD laboratory.

I appreciate the helping hands extended by my colleagues Saman Jayantha, K. Prabaharan, A. Kumar and S. Senthooran.

I will be failing in my duty, if I do not thank the Chrysler Corporation for their financial support during my stay here.

Finally, I would like to extend my thanks and gratitude to my parents for their encouragement and help to achieve this milestone in my life.

# TABLE OF CONTENTS

# ABSTRACT

Aerodynamic drag accounts for a considerable percentage of fuel consumption in commercial cargo handlers. Various experimental and computational studies were done by several researchers to find methods to reduce the drag. Front vehicle shape and the rear vehicle side modifications are suggested by various researchers over the years. The rear side optimization has generated a considerable interest among the experimental and computational aerodynamists. Fixing an inflatable boattail to the rear end of tractor trailers has been the widely used technique by fluid dynamists to reduce the drag caused by the pressure drop in the rear end.

The current study focuses on finding an optimal boattail shape using CFD techniques. Both Upwind differencing and the QUICK were used formulation with the SIMPLE algorithm to calculate the flow field around the tractor-trailer. The drag coefficients were compared with the available experimental data. The QUICK formulation closely followed the experimental values.

# LIST OF FIGURES

# NOMENCLATURE

| | |
|---|---|
| ρ | density |
| ε | dissipation rate of turbulence energy |
| μ | dynamic viscosity |
| ν | kinematic viscosity |
| φ | general variable |
| Δt | time step |
| D | boattail diameter |
| E | internal energy |
| Re | Reynolds number |
| T | Temperature |
| k | kinetic energy of turbulence |
| l | boattail length |
| p | static pressure |
| t | time |
| u | x component of the velocity |
| v | y component of the velocity |
| w | z component of the velocity |

# CHAPTER I

# INTRODUCTION

Over the years fluid dynamists have exerted a great deal of effort to reduce the drag forces on various types of automobiles. The aerodynamic drag forces on large cargo handlers has been a major concern in the design of trucks. Various studies over the years suggest that 20 percent of the total aerodynamic drag on a large bluff body is due to the low pressure region in the rear (Drollinger 1987)[2]. A considerable amount of pressure recovery can be achieved by tapering sides of a bluff body near the rear. Since rear end tapering will result in a considerable reduction in the cargo capacity, attachment of a tapered device is deemed to be desirable. Such tapered devices are referred to as boattails in the literature, hereafter the term boattail will be used to refer to the drag reducing device.

## 1.1. Importance of CFD Analysis

Computational methods have gained importance with the advent of high speed digital computers. Problems, which would have taken days to work out with the computers made in the sixties, can now be solved at very little cost in a few seconds of computer time with modern computers.

Although using wind-tunnels for measuring aerodynamic drag forces for flow past bluff bodies continues to be important, particularly where the flow involved are complex, the trend in design is clearly towards greater reliance on computer-based predictions.

The considerable increase in computing speed coupled with the improvement in numerical algorithms has rapidly decreased the cost for a given calculation. On the other hand, the cost of performing experimental studies has steadily increased. This trend in the cost does not necessarily imply that computational methods will completely replace experimental testing but it suggests that computational methods are likely to be used more extensively in the future.

Numerical simulation can be used as a tool to generate scientific understanding of the mechanisms involved in, and the behavior of flows of interest. Experiments suffer from the basic limitations like wall interference, flow angularity, and Reynolds number. Numerical flow simulations, on the other hand, have none of these limitations, but they have their own disadvantages. Numerical methods cannot produce results beyond the validity of the physical model on which the mathematical model is based. The numerical method may require excessive computer time and memory.

## 1.2. Objective

The primary objective of this study is to determine an optimal boattail shape to reduce the drag coefficient of a tractor trailer by using HEAD3D®. ICEM CFD® is used to generate the geometry and the computational mesh. Ensight® is employed to display the 3D results in pictorial form.

Further the QUICK (Quadratic Upwind Interpolation for Convective Kinematics) and upwinding difference schemes are employed along with the SIMPLE (Semi-Implicit Method for Pressure-Linked Equations) algorithm in the solver. The accuracy of both the QUICK and upwinding schemes are compared.

# CHAPTER 2

# LITERATURE REVIEW

The history of automobile aerodynamics occupies four chronologically indistinct phases. In the first phase, dating from the turn of the century, an attempt was made to design automobile shapes from procedures used in other disciplines such as naval architecture and airship engineering. Fig. 2.1 shows a vehicle in the shape of an airship and Fig. 2.2 shows a boat-like tail attachment to a car. In the second phase, post-second world war period, so-called streamlined vehicles were introduced by the German scientist Jaray and others. Figures 2.3 and 2.4. show the models developed with the streamline concept.

The method of optimizing body details developed by Hucho, Janssen and Emmelmann [13] represents the third phase. Fig. 2.5 shows the details of a body optimization technique. In body optimization, a stylistic design is made first and the modification of details such as radii, taper, spoilers, etc., are carried out wherever required. In the fourth and the current phase, unlike the detail optimization method, shape design of an automobile starts from a low-drag body with the same overall dimension as the final car. In this approach, this low-drag configuration is converted into a real car step-by-step, applying the optimization technique for each detail. Fig. 2.6 shows a typical development of a car by this technique

The need for high-speed trucks and buses arose with the construction of high-speed road systems in the 1930s. The rear end optimization of trucks and buses started with models based on the ideas of Jaray (Fig. 2.7) and Kamm (Fig. 2.8).

4
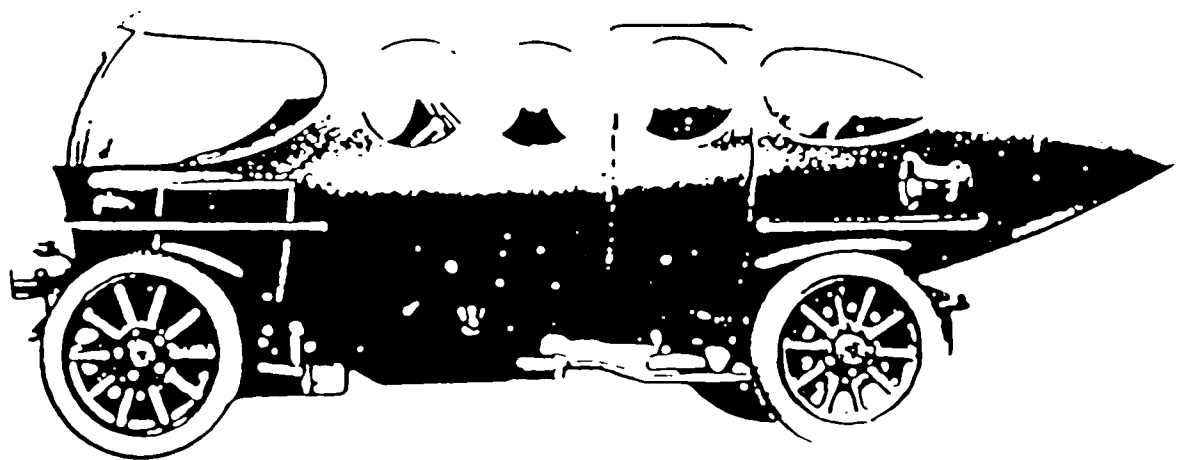
Fig. 2.1. Alfa Romeo of Count Ricotti, 1913
(Reproduced from [13])
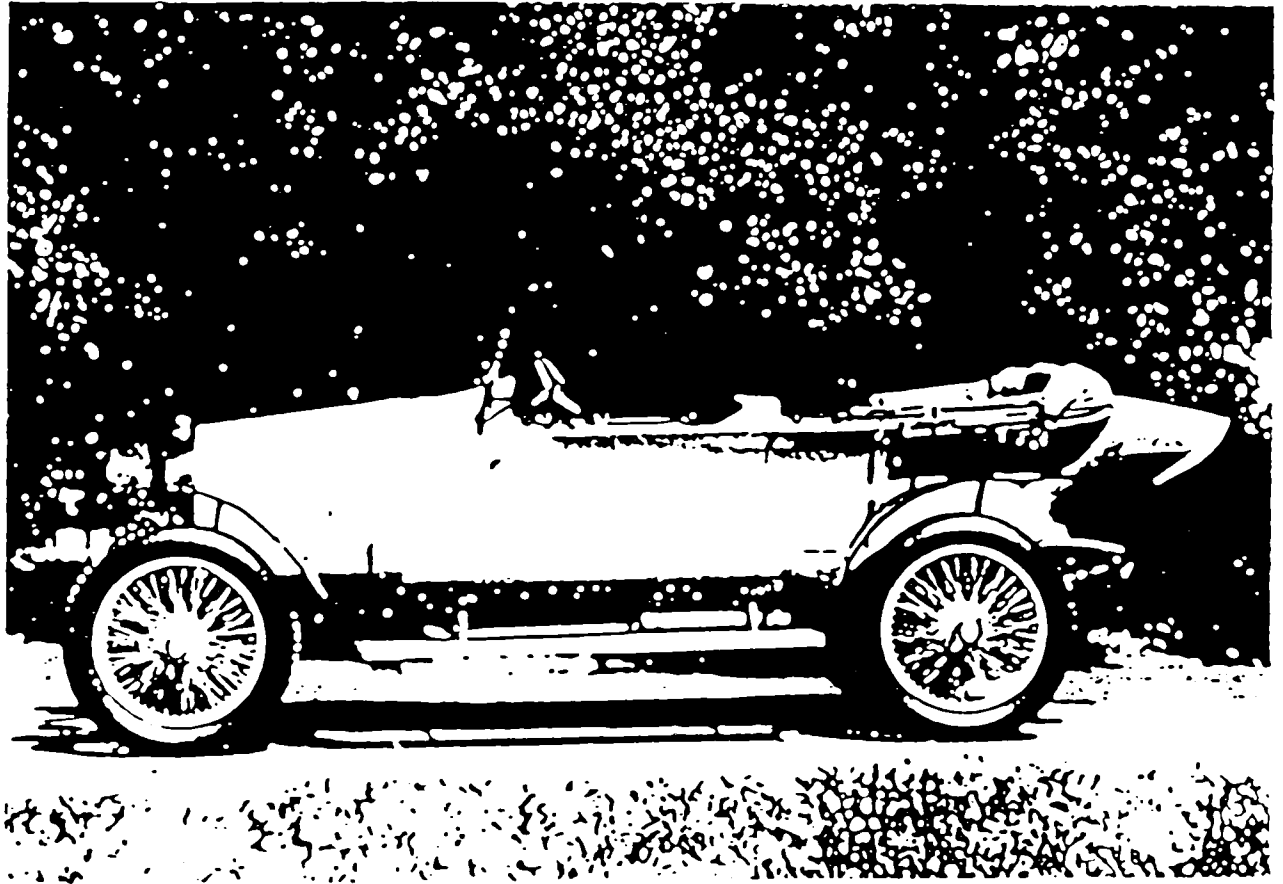
Fig. 2.2. Boat-tailed 'Audi Alpensieger', 1913
(Reproduced from [13])
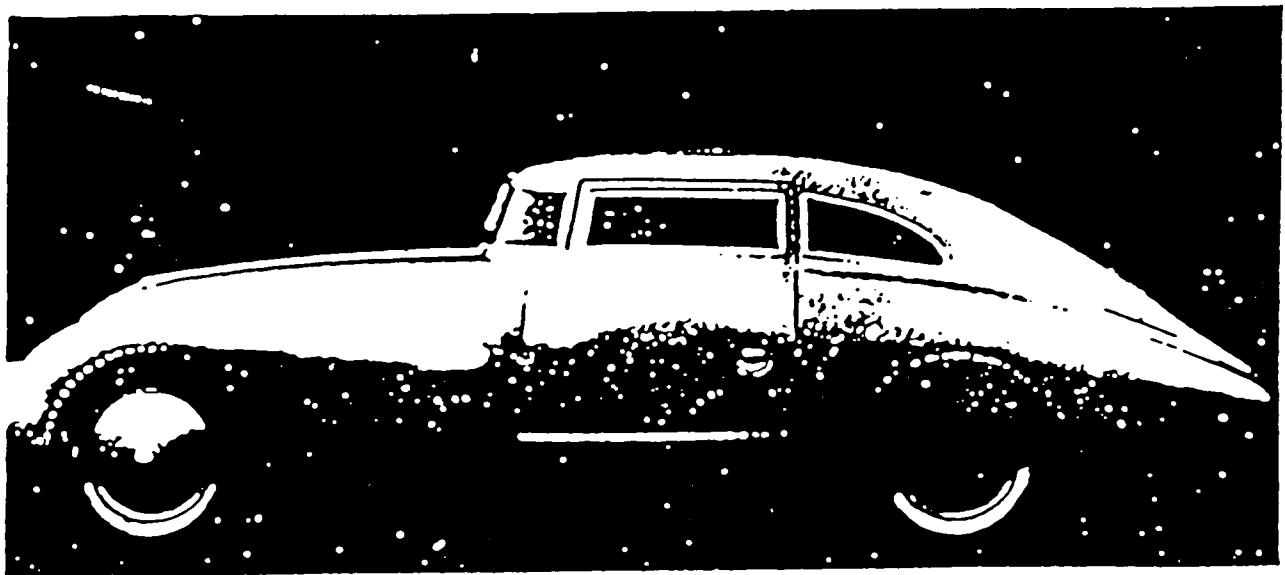
Fig. 2.3. The 1.5 litre Adler-Trumpf, 1934/35
(Reproduced from [13])
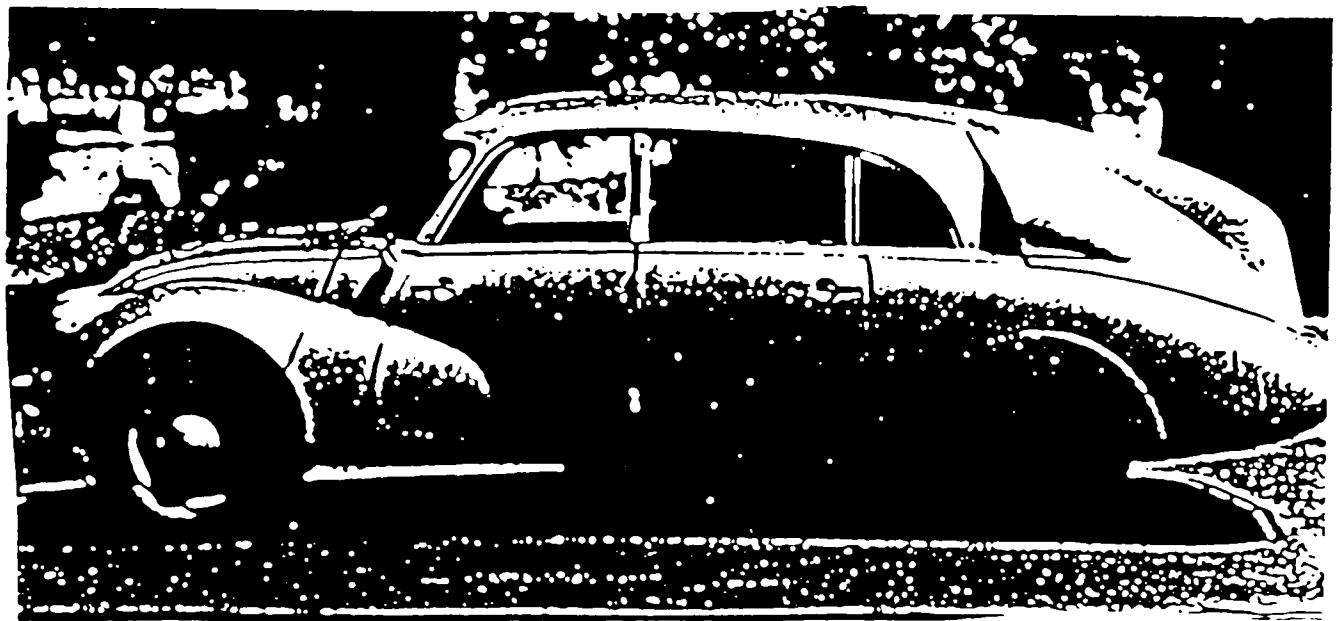
Fig. 2.4. The 3-litre 8-cylinder Tatra Type 87
(Reproduced from [13])

Fig. 2.5. Optimization of body details
(Reproduced from [13])

9

Fig. 2.6. Development of a low drag body from a basic shape
(Reproduced from [13])

Fig. 2.7 Jaray bus rear end design
(Reproduced from [13])

Fig. 2.8. Kamm bus rear end design
(Reproduced from [13])

For large bluff bodies, 20 percent of the aerodynamic drag is due to low pressure at the rear. The focus of this study is to investigate the drag reduction achievable through the introduction of an inflatable boattail in large bluff bodies at the rear end. The basic principle underlying this concept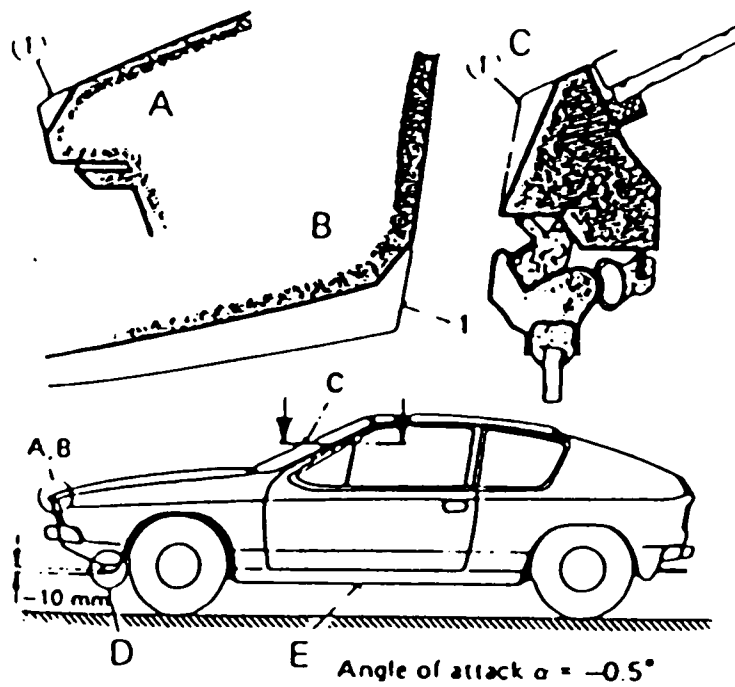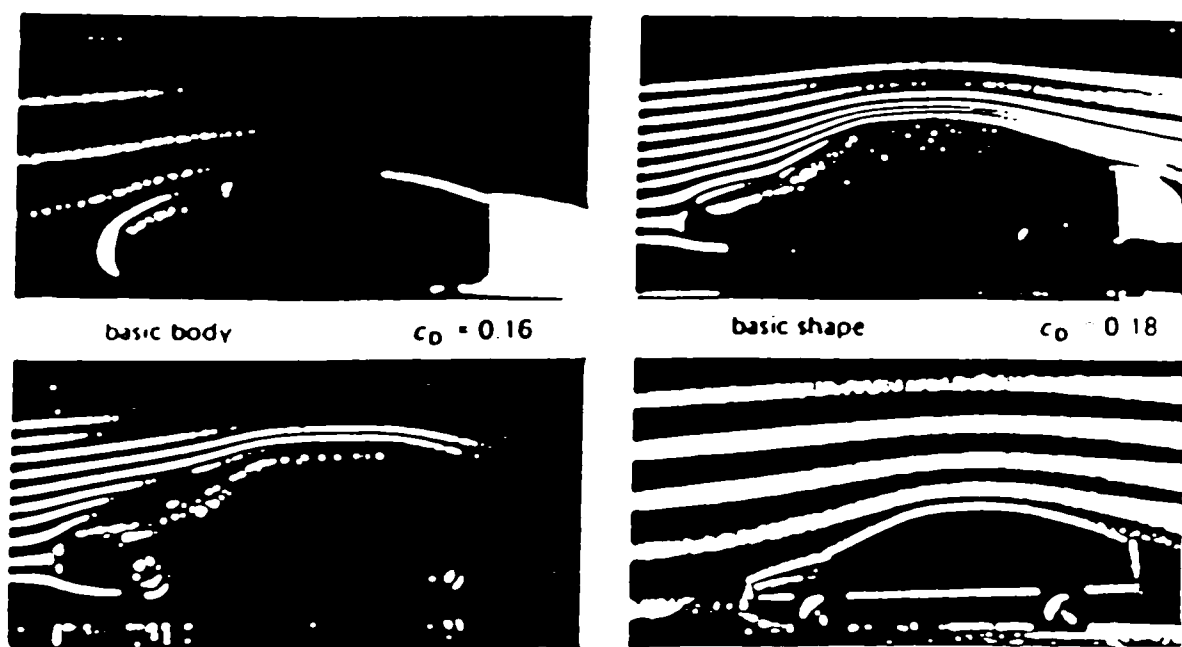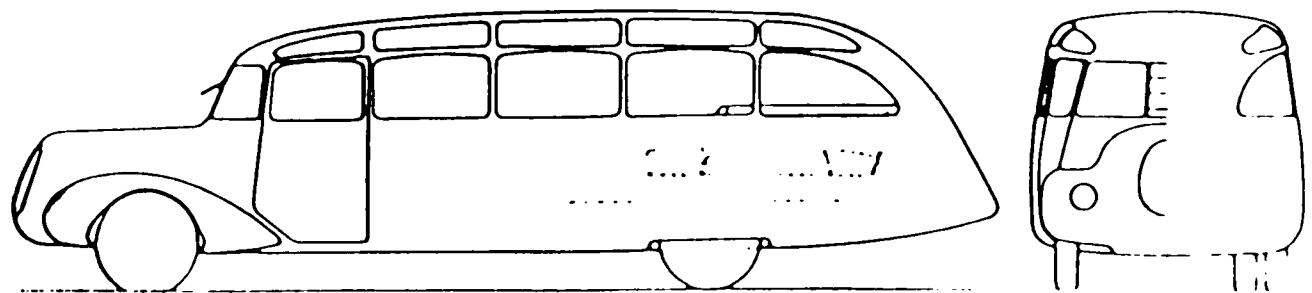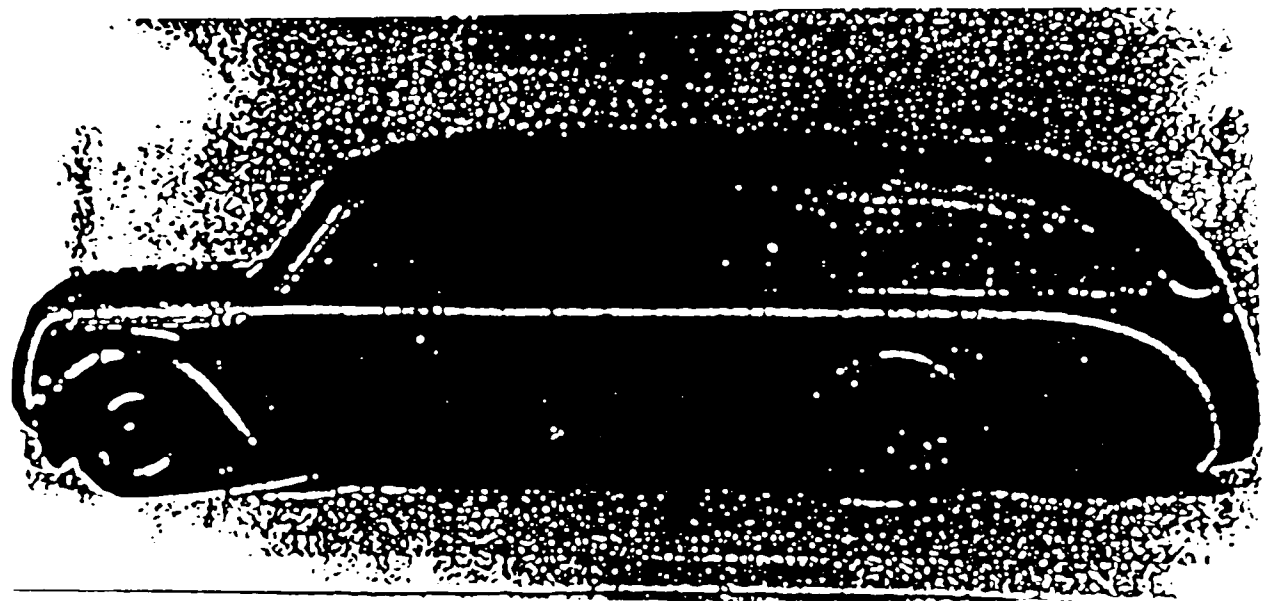 is that "By gradually tapering the body the flow is subjected to a pressure increase at the rear of the vehicle, the 'base pressure' is comparatively high, which it self then reduces the drag" [13], p.13.

Various studies has been done experimentally and numerically to find an optimum boattail shape. In 1981, Peterson [12] developed an optimum boattail shape by modifying a full-scale box-shaped vehicle with rounded corners and an enclosed underbody. He reported a drag reduction of 32 percent with a full boattail and 31 percent with a truncated boattail.

Han [4] conducted a three-dimensional numerical investigation to optimize the rear end of a vehicle-like body in ground proximity. Nine different combinations of the three shape parameters, namely boat-tail angle, backlight angle and ramp angle, were considered. The boattail angle is the angle seen from the top view. The backlight angle is the top angle as seen from the side view, whereas the ramp angle is the bottom angle as seen from the side view. Han observed that the optimum after-body shape minimized the trailing vortices in the wake and also produced near zero after-body lift forces. Their optimum design geometry for the backlight, boat-tail and ramp angles were 17.8, 18.9 and 9.2 degrees, respectively. The reported drag coefficient reduction was 0.13

Hassan [5] in 1995 conducted a numerical study to optimize an inflatable boattail geometry to reduce the aerodynamic base drag on standard class-8 tractor trailer configurations. Conical, ogival and elliptical boattails of 5 and 8 feet lengths were considered. They concluded that the boattails reduced the drag by 9 and 12.7 percent for the 5 and 8 feet boattails, respectively.

Funderburk [3] investigated Hassan's work experimentally for the 5 feet length boattail and found a drag reduction in the order of 10 percent. The 5 feet length was considered in accordance with the current US Federal law on US high ways.

# CHAPTER 3

# THEORETICAL FORMULATION

This chapter presents the equations to be solved for the current study, their numerical formulation and an brief account of the algorithm used to solve the governing equations. This chapter also include a discussion on the incompressible three-dimensional flow solver, HEAD3D®, developed by S. Parameswaran. This code uses the standard k-ε model of Launder and Spalding [7] and the modified SIMPLE algorithm of Patankar and Spalding [10]. For this study the QUICK algorithm of Leonard [8] was incorporated as an additional differencing scheme along with the existing upwinding scheme.

## 3.1. Governing equations

The flow around an automobile is highly turbulent and unsteady. The Airflo3d® code is used to solve the Navier-Stokes equation. The governing equations for the flow field in the Cartesian tensor notation is as follows.

Continuity Equation

$$\frac{\partial U_i}{\partial x_i} = 0$$

Momentum Equation

$$\frac{\partial U_i}{\partial t} + \frac{\partial}{\partial x_j}\left(U_i U_j\right) = -\frac{1}{\rho}\frac{\partial p}{\partial x_i} + \frac{\partial}{\partial x_j}\left\{ v_{eff}\left(\frac{\partial U_i}{\partial x_j} + \frac{\partial U_j}{\partial x_i}\right)\right\}$$

The term $\nu_{eff}$, the effective kinetic viscosity, is the sum of molecular viscosity and turbulent viscosity

$$\nu_{eff} = \nu + \nu_t,$$

Energy Equation

$$\rho \frac{du}{dt} = \nabla \cdot (k\nabla T) + \phi.$$

Here u is mean velocity, T is mean temperature, $\rho$ is density, p is pressure and t is time.

The kinematic viscosity, $\nu_t$, is obtained from the standard k-$\varepsilon$ model as follows

$$\nu_t = \frac{C_\mu k^2}{\varepsilon},$$

Where $C_\mu$ is the model constant and k and $\varepsilon$ are turbulent kinetic energy and its rate of dissipation. The quantities k and $\varepsilon$ are obtained by solving the following partial differential equations, see Ref. [7].

The k equation

$$\frac{\partial k}{\partial t} + \frac{\partial}{\partial x_j}(u_j k) = \frac{\partial}{\partial x_j}\left(\frac{\nu_t}{\sigma_k}\frac{\partial k}{\partial x_j}\right) + G - \rho\varepsilon.$$

The $\varepsilon$ equation

$$\frac{\partial \varepsilon}{\partial t} + \frac{\partial}{\partial x_j}(u_j \varepsilon) = \frac{\partial}{\partial x_j}\left(\frac{\nu_t}{\sigma_\varepsilon}\frac{\partial \varepsilon}{\partial x_j}\right) + \frac{\varepsilon}{k}(C_1 G - C_2 \varepsilon).$$

Here

$$G = \nu_t \frac{\partial u_i}{\partial x_j}\left(\frac{\partial u_i}{\partial x_j} + \frac{\partial u_j}{\partial x_i}\right)$$

and $C_1 = 1.44$, $C_2 = 1.92$, $C_\mu = 0.09$, $\sigma_k = 1.0$, $\sigma_\varepsilon = 1.22$ are empirical constants

## 3.2. Numerical formulation

The numerical formulation of this problem is primarily based on the

SIMPLE (Semi-Implicit Method for Pressure-Linked Equations) algorithm of

Patankar and Spalding [10]. The grid formulation employed in the HEAD3D®

program is shown in Figure 3.1. It shows the vertices' numbering and the

nomenclature used for faces.

In the HEAD3D® solver, the momentum equation is discretized as given

below.

$$\rho Vol_p \frac{\left(\phi_p^{n+1} + \phi_p^n\right)}{\Delta t} + \left(F_1^n \phi^{n+1}\right)_e - \left(F_1^n \phi^{n+1}\right)_w + \left(F_2^n \phi^{n+1}\right)_n - \left(F_2^n \phi^{n+1}\right)_s$$

$$+ \left(F_3^n \phi^{n+1}\right)_t - \left(F_3^n \phi^{n+1}\right)_b = \left(\frac{a^2}{Vol}\right)_e \left(\phi_e^{n+1} - \phi_p^{n+1}\right) - \left(\frac{a^2}{Vol}\right)_w \left(\phi_p^{n+1} - \phi_w^{n+1}\right)$$

$$+ \left(\frac{a^2}{Vol}\right)_n \left(\phi_n^{n+1} - \phi_p^{n+1}\right) - \left(\frac{a^2}{Vol}\right)_s \left(\phi_p^{n+1} - \phi_s^{n+1}\right)$$

$$+ \left(\frac{a^2}{Vol}\right)_t \left(\phi_t^{n+1} - \phi_p^{n+1}\right) - \left(\frac{a^2}{Vol}\right)_b \left(\phi_p^{n+1} - \phi_b^{n+1}\right)$$

$$+ S_\phi \cdot Vol_p$$

Where $F_1$, $F_2$ and $F_3$ are the convective fluxes across the east, north and top

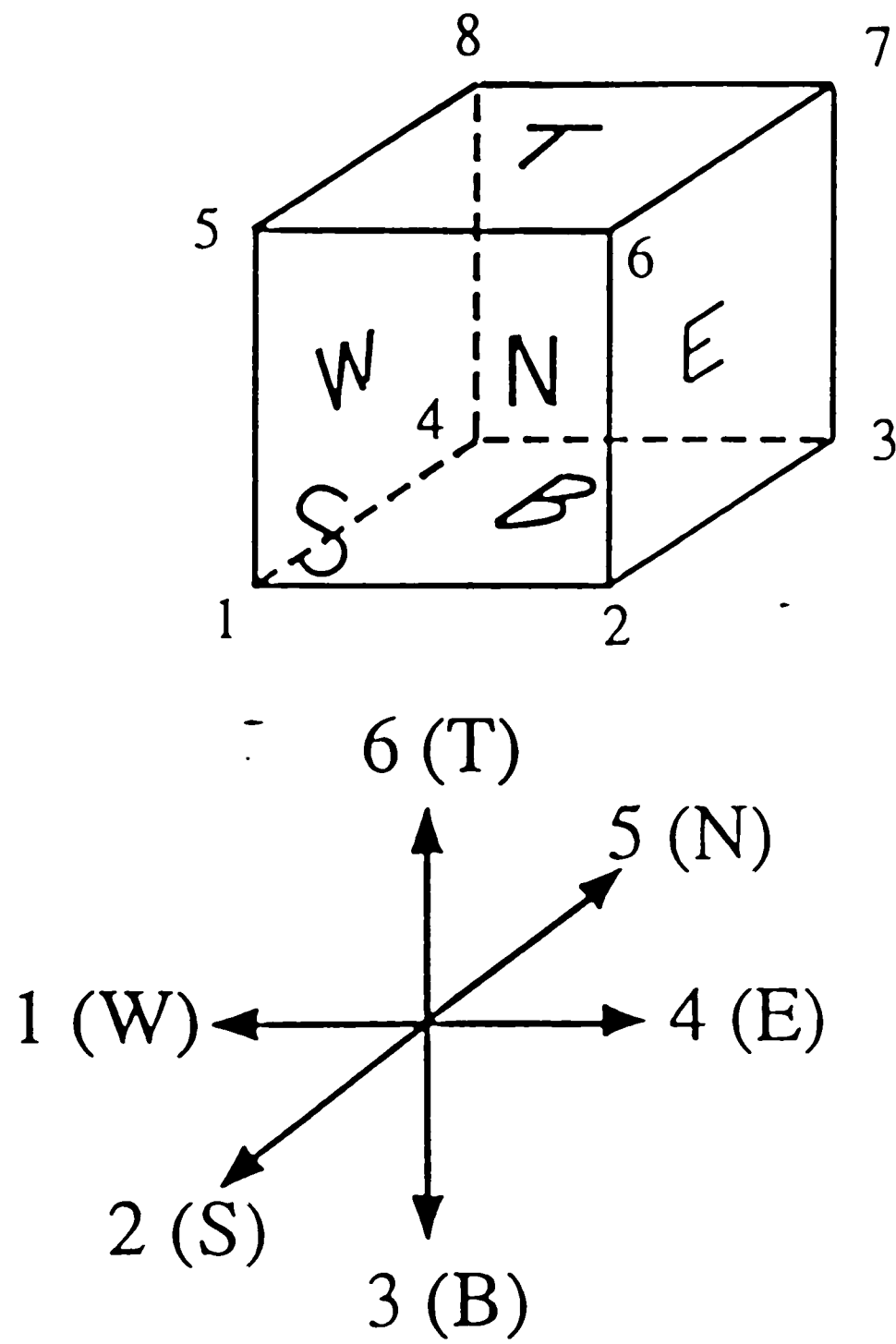faces, a is the area of any of the six cell faces and Vol. is the volume of a general

cell.

Fig. 3.1. Three-dimensional Grid layout

In the standard HEAD3D$^\text{®}$ program, upwind differencing scheme is employed in discretizing the convective terms. For this study, QUICK formulation by Leonard [8]is added as a subroutine and the results are obtained for both cases. Now let us consider these two schemes in one-dimensional form for simplicity. Fig. 3.2 provides the basis of a one-dimensional control volume formulation for the transport of the scalar quantity $\varphi$.

### 3.2.1. Upwind differencing

The first-order upwinding used in this study defines the value of $\varphi$ in the east face as follows:

$$\phi_e^{n+1} = \phi_P^{n-1} \quad \text{if } F_1^n > 0$$
$$= \phi_E^{n+1} \quad \text{if } F_1^n < 0$$

### 3.2.2. QUICK Formulation

The QUICK scheme employs a three-point upstream weighted quadratic interpolation technique to compute the convective quantity. In the QUICK formulation, the value of $\phi$ at the east face is given by:

$$\phi_e = \phi_P + \frac{p_1}{2}(\phi_E - \phi_P) - \frac{p_2}{3}(\phi_E - 2\phi_P + \phi_w) \quad \text{if } F_1^n > 0$$

$$\phi_e = \phi_E + \frac{p_1}{2}(\phi_P - \phi_E) - \frac{p_2}{3}(\phi_P - 2\phi_E + \phi_{EE}) \quad \text{if } F_1^n < 0$$
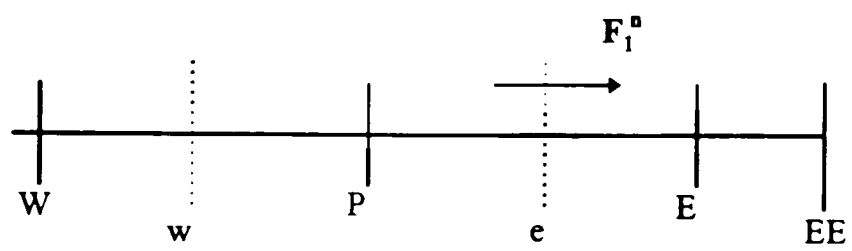
here p1=1, p2=0.375.

19

Fig. 3.2. One-dimensional grid layout

## 3.3. Solution procedure

In HEAD3D®, the solution to the coupled momentum and continuity equations is obtained by carrying out the following steps:

1. Store results of previous time step; update viscosity and terms related to wall functions.

2. Obtain Cartesian components from old pressure. Solve the velocity projections at the cell faces explicitly from momentum balance.

3. Compute the continuity error for each cell from the velocity projections.

4. Correct the pressure and the velocities until the momentum and continuity equations are satisfied.

5. Compute the turbulence production rate.

6. Solve for the turbulence kinetic energy, k, and dissipation rate $\varepsilon$.

Take a new step and repeat steps (2) to (5) until steady state is achieved.

# CHAPTER 4

# PREPROCESSING

The geometry creation, grid generation and creating the data files for a given solver are the main steps in preprocessing. In this study, ICEM CFD®, a commercial preprocessor, is used to create the mesh.

## 4.1. Tasks in preprocessing

In preprocessing, one has to perform the following tasks:

1. Create the geometry.

2. Define the control volumes for which the conservation laws are applied and apply the boundary conditions.

3. Specify the initial condition and set the fluid properties.

4. Set the Numerical control parameters.

5. Writing the output data files in an HEAD3D® readable format.

### 4.1.1. Geometry Creation

The module DDN in the software is used to create the geometry. The module MULCAD, used to create the mesh, can only use lines and B-spline curves as edge entities. So all the non-B-spline curves must be converted to B-spline curves before proceeding to create the mesh with the module MULCAD. The B-spline surfaces also have to be converted in the same way.

When creating the geometry the topology must be decided and the corresponding lines and B-spline curves have to be drawn. The HEAD3D$^\varepsilon$ , ICEM CFD$^\circledR$ interface, is devised to generate an internally structured mesh. Hence the geometry lines must be drawn in such a way that domains can be created with module MULCAD. Inside every domain, one can draw consistent **ijk** directions thus giving an internally structured mesh within each domain.

4.1.2. Defining the control volumes and specifying boundary conditions

Before creating the control volumes at a finer level, the sub-faces and the domains have to be created. The domain pattern employed in this study is shown in Fig. 4.1 and Fig. 4.2 . When selecting a domain, grid layout must be the main consideration because a well-planed domain will result in a better grid layout.

After creating the domain, the number of nodes per master edges have to be decided. Though there is not much restriction on this phase, a user must use his own judgment in creating an evenly spaced mesh, otherwise the program would take much time to converge. The grid layout is shown in Figures 4.3, 4.4, 4.5 and 4.6 .

Finally, one has to specify the boundary conditions. In this study, wall, symmetric plane, velocity inlet and velocity exit are the main boundary conditions. The boundary conditions can be assigned by clicking the respective sub-faces on the geometry.

4.1.3. Specifying the initial condition and setting the fluid properties.

The initial conditions are specified before writing out the data files to run with the HEAD3D®. In this study, the initial velocity was the main concern and one has to specify a good guess in the corresponding directions. Since the study is done with a Reynolds number of 4.2E5, Reynolds numbers for all the cases' fluid properties remain same.

4.1.4. Setting the numerical control parameters

The parameters controlling the HEAD3D® programs are time step, final time, number of steps, pressure convergence and velocity residuals. When specifying the time step, the Courant number must be less than or equal to one.

$$\textbf{Courant number} = \frac{\textbf{velocity inlet * time step}}{\textbf{minimum cell size in the flow direction}}$$

4.1.5. Writing the data files

The mesh data created by the ICEM CFD® has to be written in a format that could be read by HEAD3D® program. The interface program incorporated in the ICEM CFD® will write the file in either ASCII or binary format.
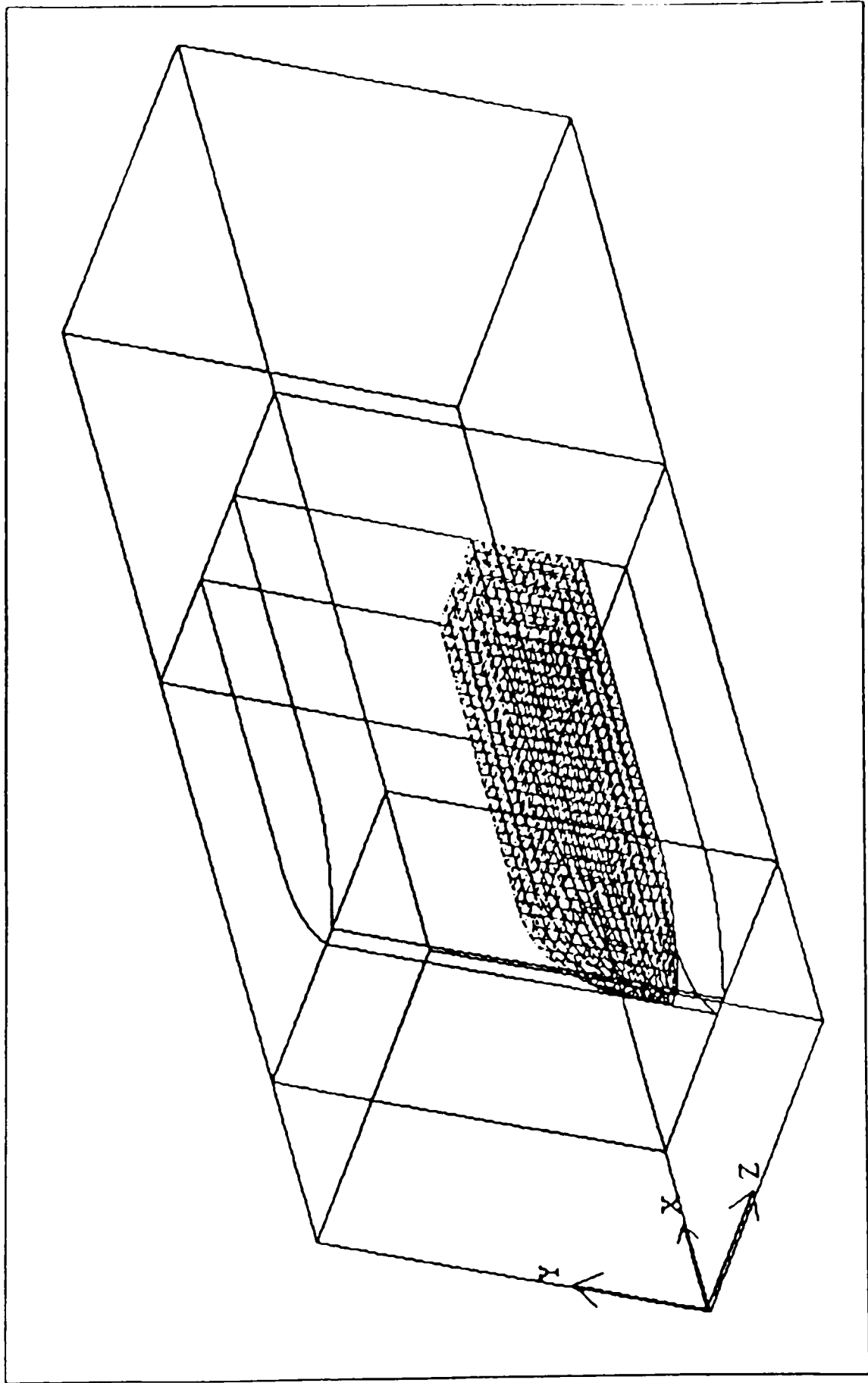
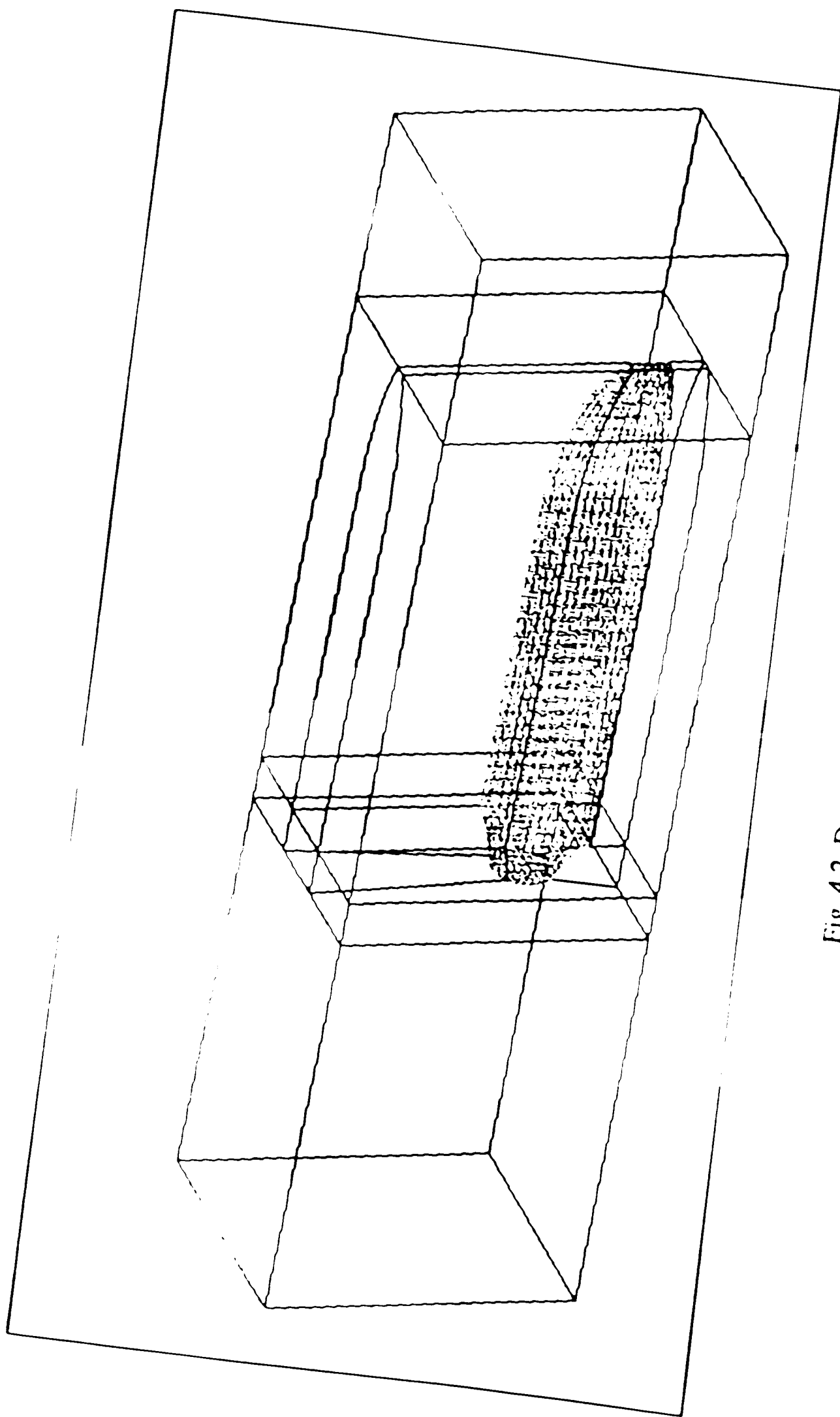Fig. 4.1. Domain lay out for truck without boattail

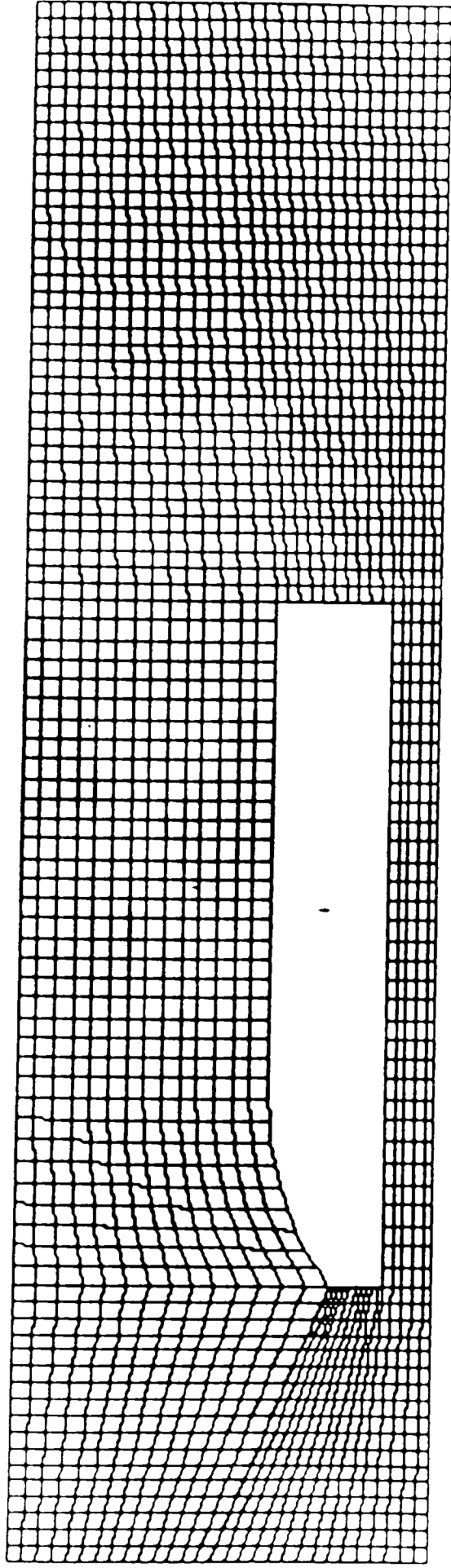Fig. 4.2. Domain layout for truck with boattail

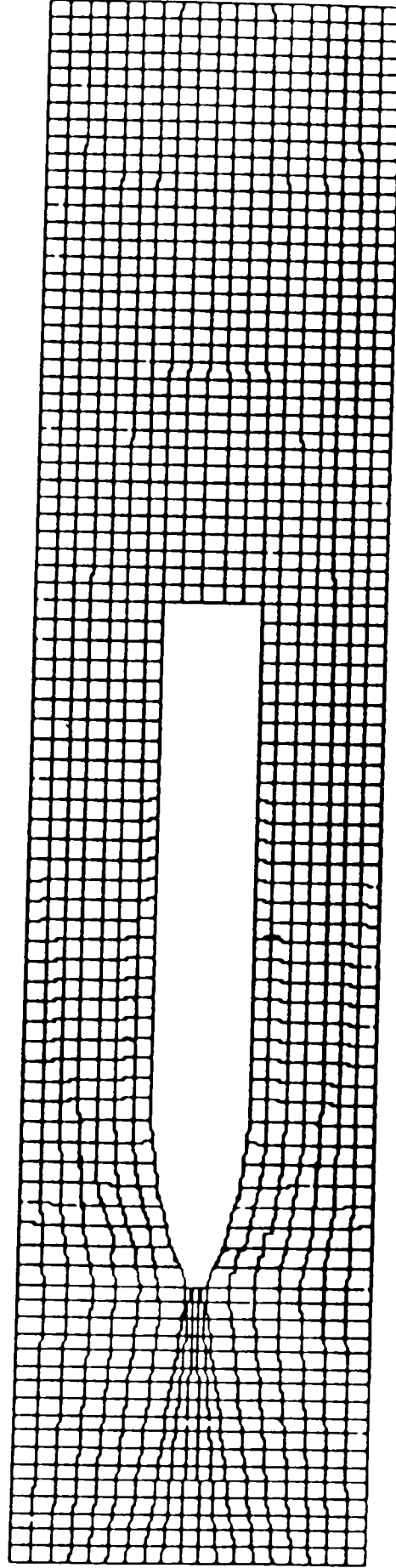Fig. 4.3. Grid layout for truck without boattail- front view
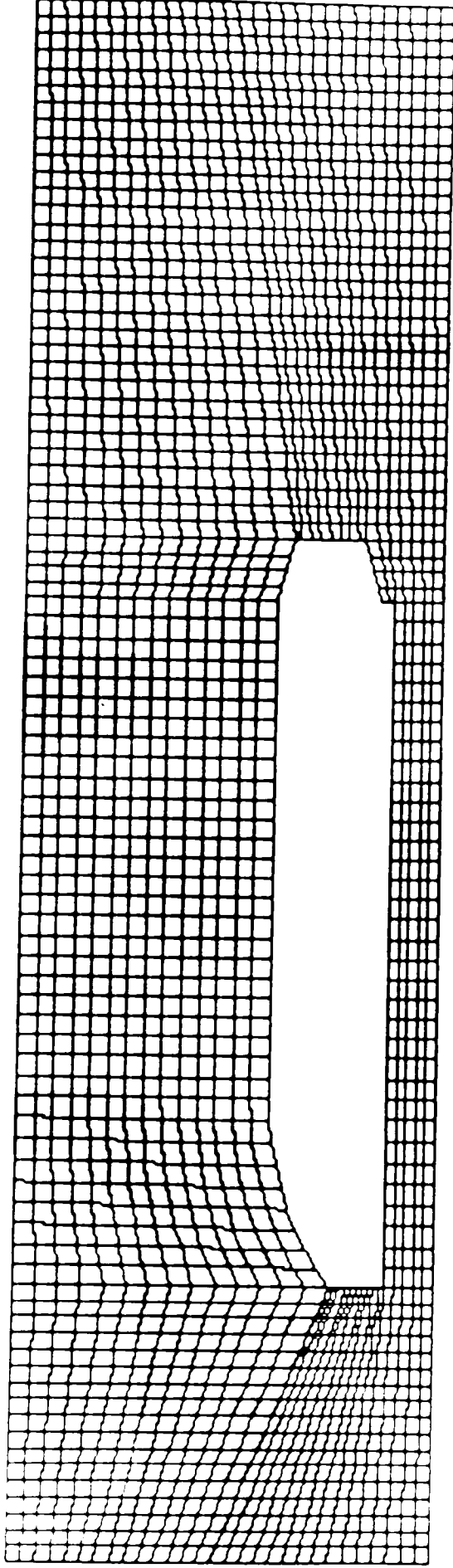
Fig. 4.4. Grid layout for truck without boattail -top view
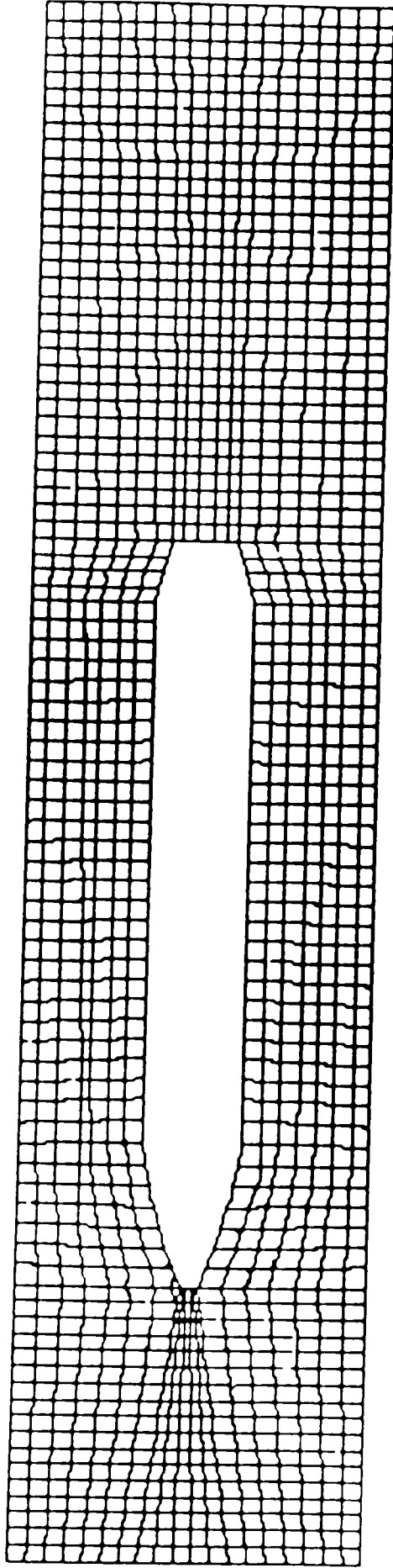
Fig. 4.5. Grid layout for truck with boattail- front view

Fig. 4.6. Grid layout for truck with boattail- top view

# CHAPTER 5

## POSTPROCESSING

The general CFD analysis creates a bulk amount of data which is hard to interpret by mere looking at numbers. It is even more difficult when dealing with the three-dimensional computations with many variables. This difficulty has paved the way for numerous postprocessing software packages in the market. The software employed in this study is Ensight®.

Ensight® is a highly advanced postprocessing software with numerous features. Velocity vector plots, pressure contours, particle trace and velocity contours can be generated with this tool. Velocity vector plots and particle traces will help to locate any recirculation region encountered in the analysis. The desired plots such as vector arrows, pressure contours and velocity profiles can be obtained in different planes by creating clip planes at desired locations.

The animation feature in the program enables one to do the flow visualization and check the validity of the solver. Whenever results are inconsistent with the experimental results, the flow visualization will help one to locate the possible error in the program.

The output file obtained from the HEAD3D® program must be converted to Ensight® readable format. A FORTRAN program, airflo3d_ensight.f, converts the output file into an Ensight® readable format. This program will generate the geometry file and results file for velocity, pressure and turbulence energy.

# CHAPTER 6

## GEOMETRY OF THE MODEL

The basic test model considered was similar to the one used by Funderburk [3] in his experimental studies. Figures 6.1 and 6.2 show the isometric view of the test model with and without boattail. Fig. 6.3 shows the enlarged view of the boattail. The length of the boattail was kept constant and the diameter (D) was changed. Figures 6.4 and 6.5 show the geometric parameters.

This study was conducted with the dimensions of a 1/5th-scale tractor-trailer model. The model was simplified and details such as the tractor-to-trailer gap, wheels and the rear crash bar were omitted. The boattail geometry of the present study was originally developed by Hassan [5], and it was termed as ogive shape. The boattail is square at the base of the trailer and transcended to a circle at the end.

The model used by Funderburk [3] was curved along the edges from the base to the circle and was also tangent to the trailer. However due to some software limitations, the current boattail shape has four sharp lines connecting the square base to the circle with a curved surface (Fig. 6.3). The boattail was not perfectly tangent to the truck.

The base diameter was the varying parameter. By changing the base diameter, the overall shape could be altered proportionally. Five different diameters 4, 5, 6,7 and 8 ft. were used to find an optimal boattail shape. The corresponding model diameters were 8.5, 10.56, 12.7 , 14.75 and 17 inches.

Throughout the study, the Reynolds number of $4.45 \times 10^5$ was maintained by adjusting the kinematic viscosity in the program. In calculating the Reynolds number, the height of the truck 20.5 inches was used as the characteristic length. The maximum cross sectional area 20.5x18.0 inches was used in calculating the drag forces.
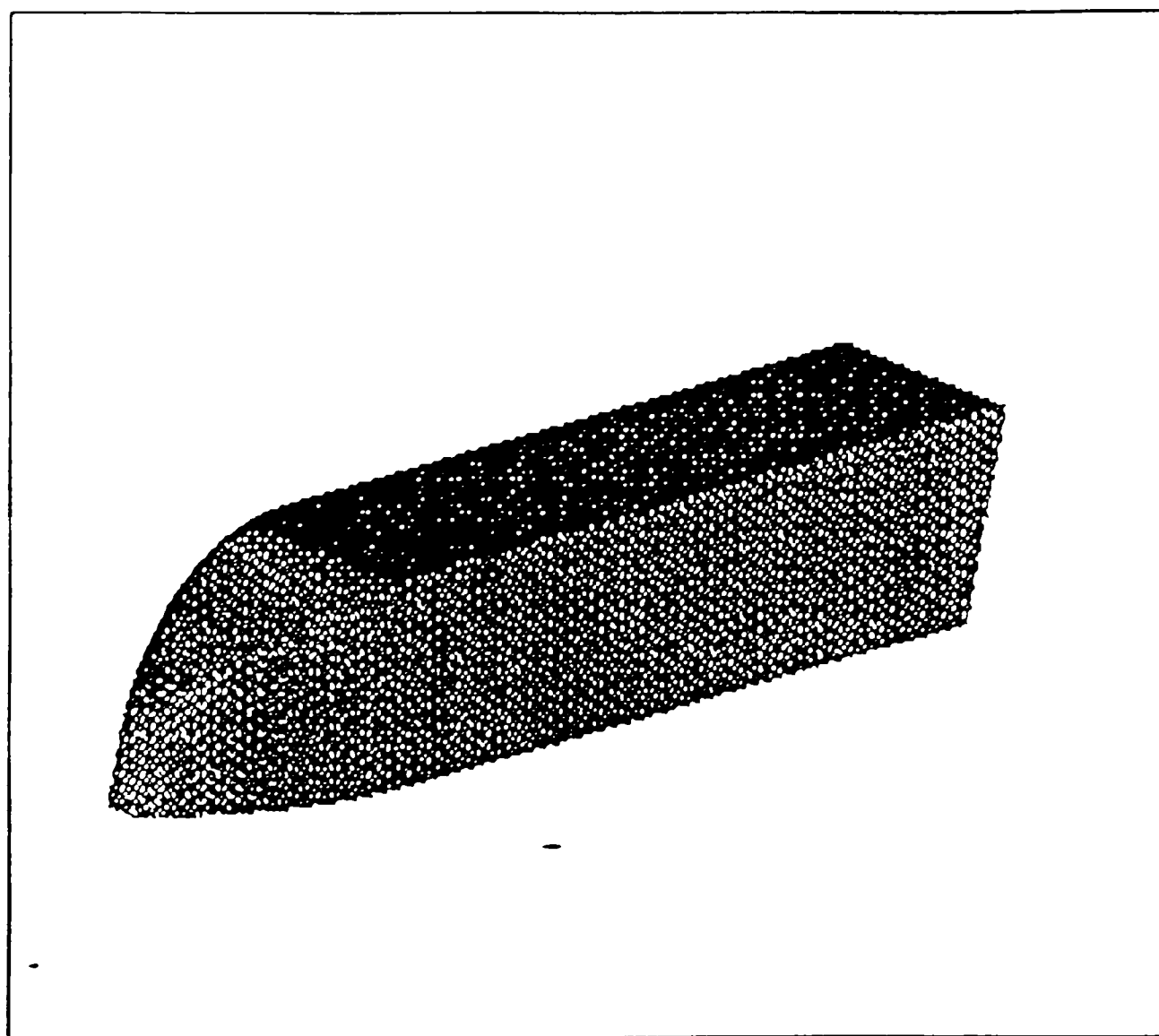
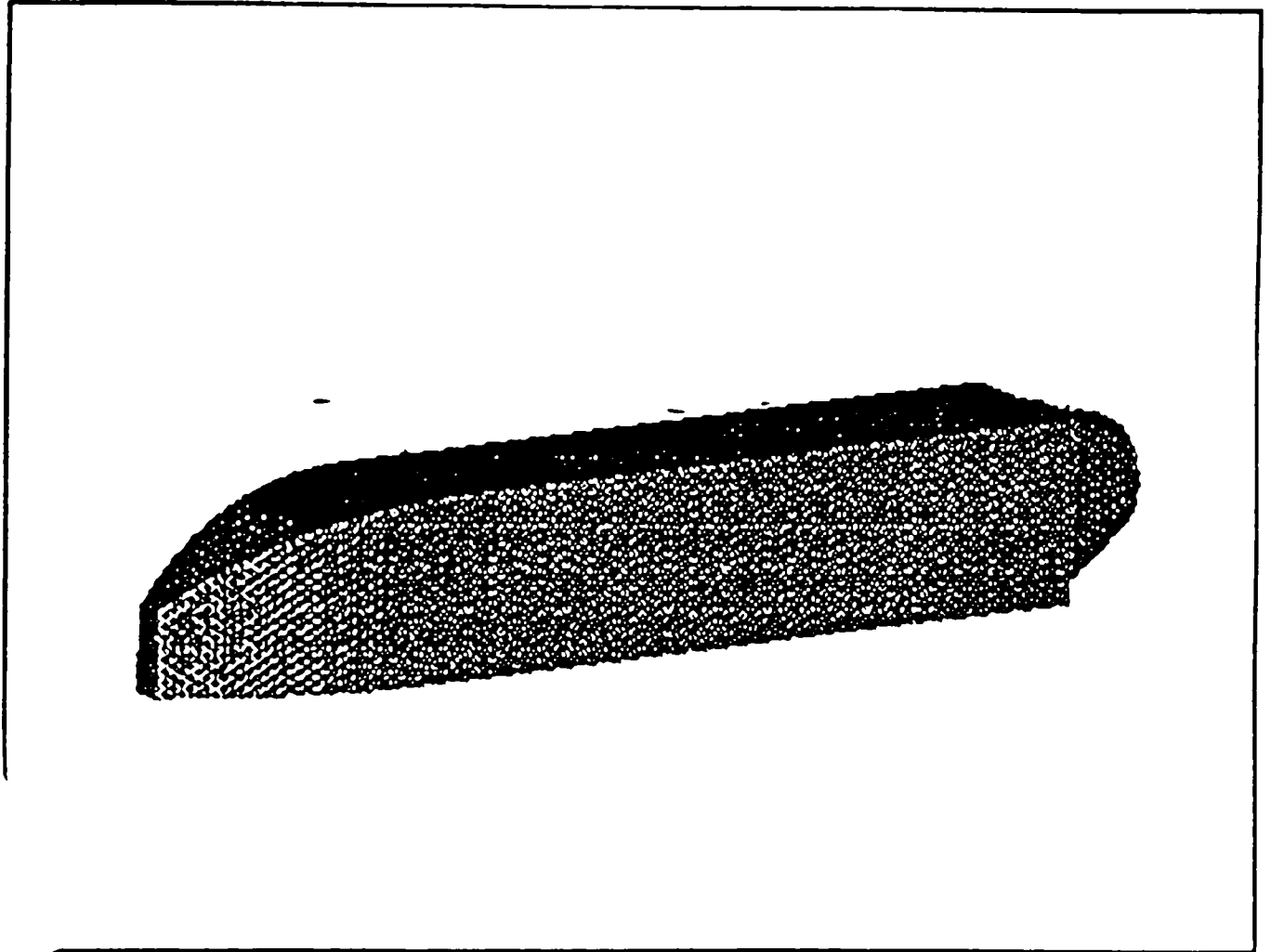Fig. 6.1 Isometric view of the truck without boattail

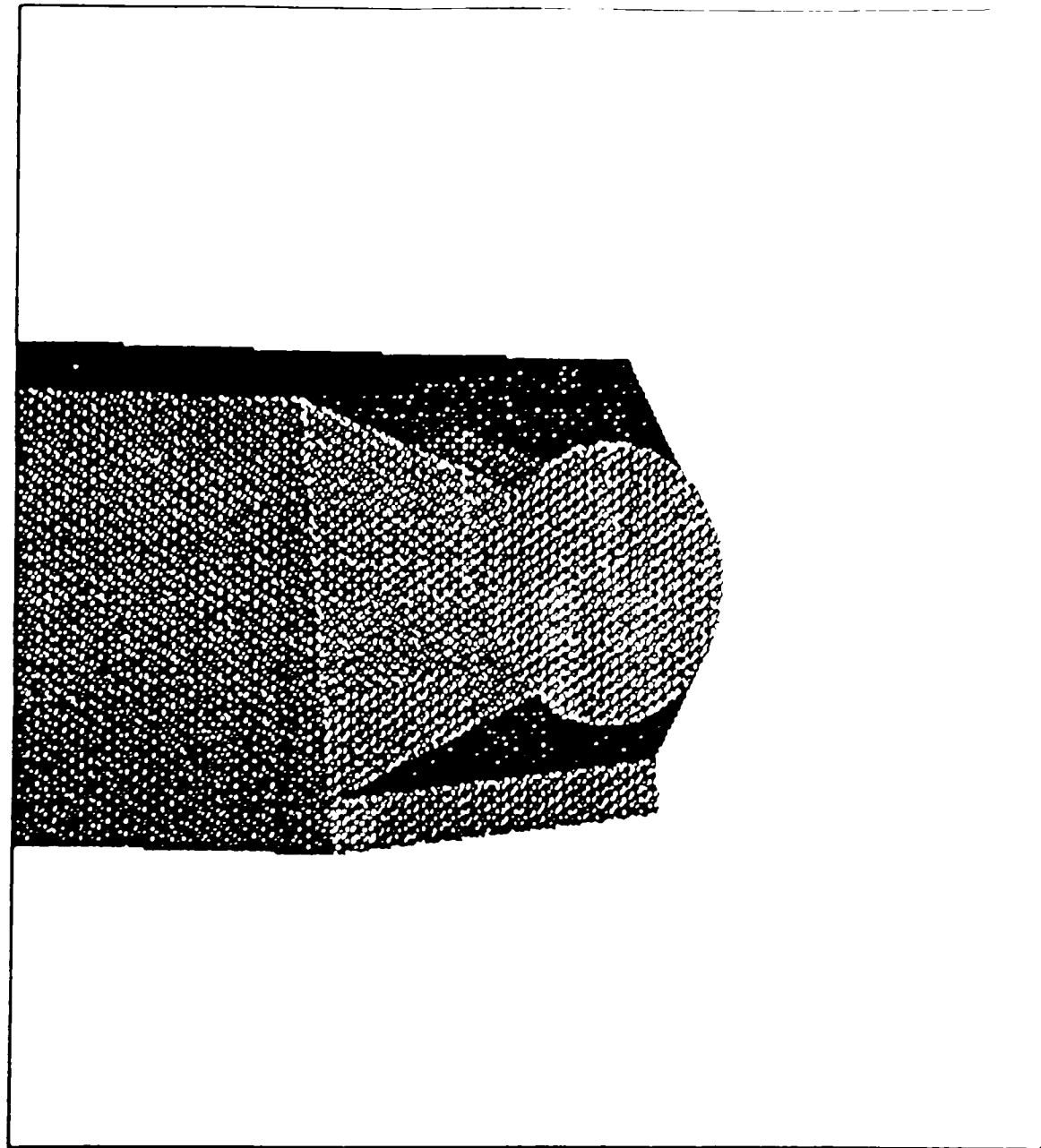Fig. 6.2. Isometric view of the truck with a boattail
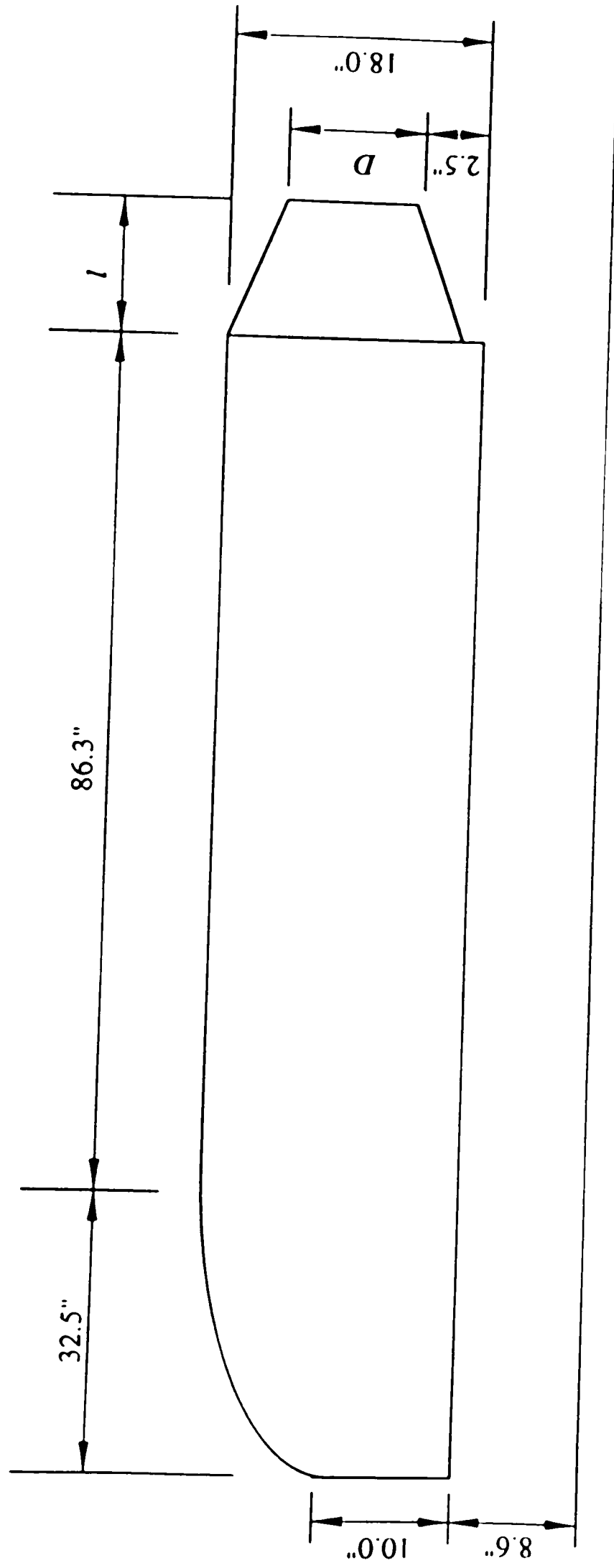
Fig. 6.3 Enlarged view of the boattail

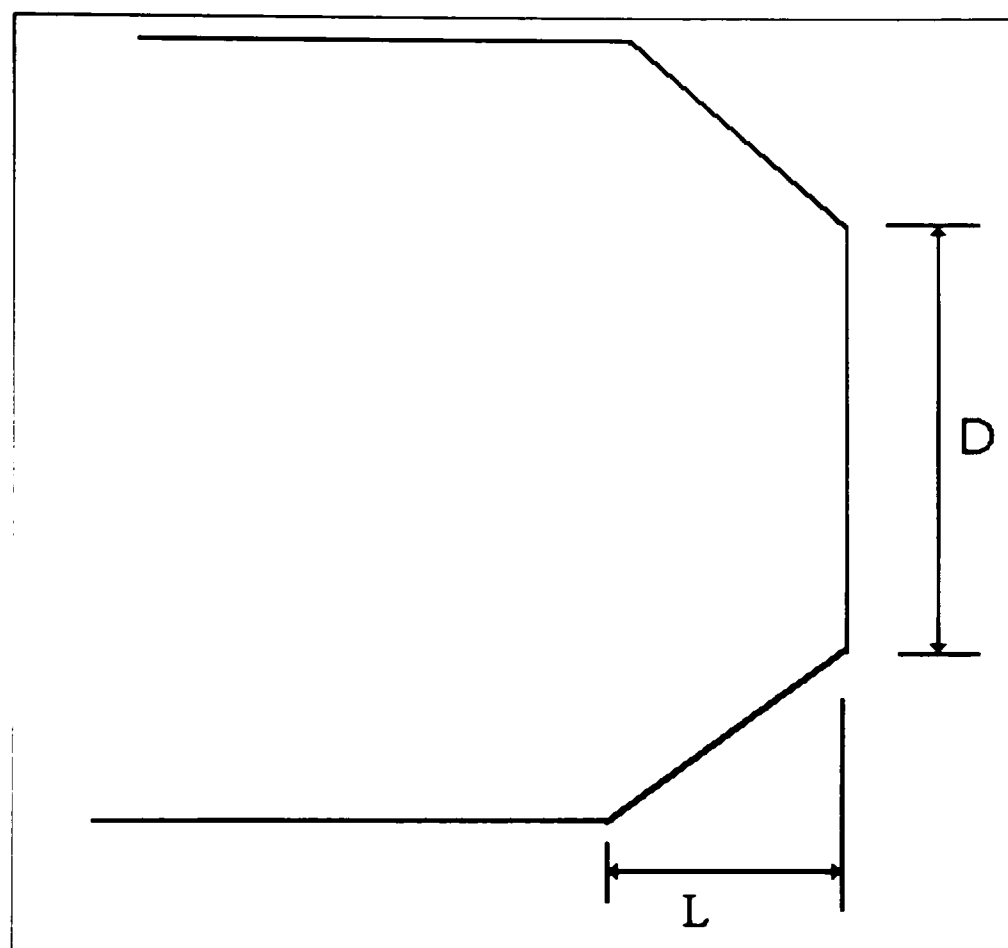Fig. 6.4. 1/5<sup>th</sup> scale tractor-trailer model

Fig. 6.5. Boattail parameter details

# CHAPTER 7

## RESULTS AND CONCLUSIONS

The main objective of this study is to find an optimal boattail shape to reduce the drag in tractor-trailers. Five different boattail diameters were used with the length of boattail kept constant at 5 ft., maximum length allowed by the Federal Regulations for US highways. The Reynolds number was kept constant at $4.35 \times 10^5$ for all the calculations.

In each case 45,526 elements were used to maintain consistency. For all boattail configurations and the non-boattail case, HEAD3D program was executed for 75 steps with upwinding and QUICK formulation. The time step was set to be $2 \times 10^{-2}$ in all cases. In all cases, the maximum residuals for the velocities were reduced to $2 \times 10^{-5}$.

The drag coefficients obtained with QUICK formulation were consistent with the results obtained by Funderburk [3]. However the standard upwind differencing tends to underpredict the drag forces. Fig. 7.1 and Table 7.1 show the results of experimental, upwinding and the QUICK scheme.

The vector arrows (Figures 7.11-7.14) and particle traces (Figures 7.2- 7.6) are consistent with standard flow phenomena. The particle traces clearly demonstrate a considerable reduction in flow separation when the boattail is introduced. The wake behind the trailer without a boattail is characterized by a large separation zone as shown in Fig. 7.11. At the symmetric plane two recirculating vortices are clearly visible.

Table 7.1. Drag coefficients for different configurations

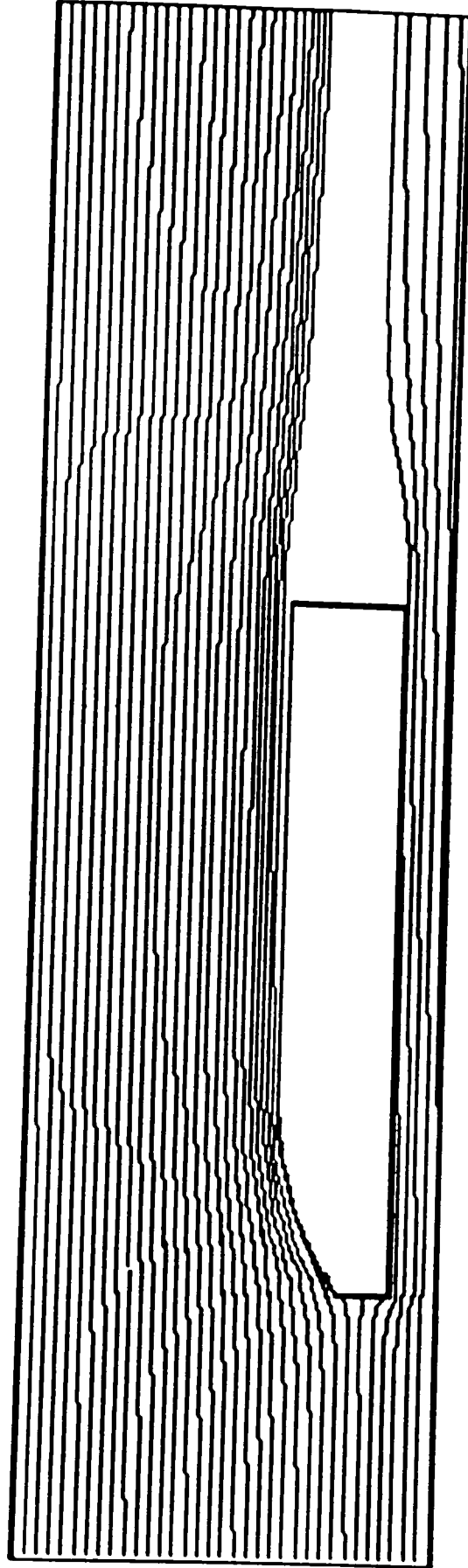| Configuration | Experimental | QUICK | Upwinding |
|---|---|---|---|
| Without boattail | 0.47 | 0.514 | 0.502 |
| Boattail-1 | 0.46 | 0.464 | 0.448 |
| Boattail-2 | 0.46 | 0.478 | 0.409 |
| Boattail-3 | 0.45 | 0.453 | 0.344 |
| Boattail-4 | 0.43 | 0.436 | 0.358 |
| Boattail-5 | | 0.521 | 0.407 |
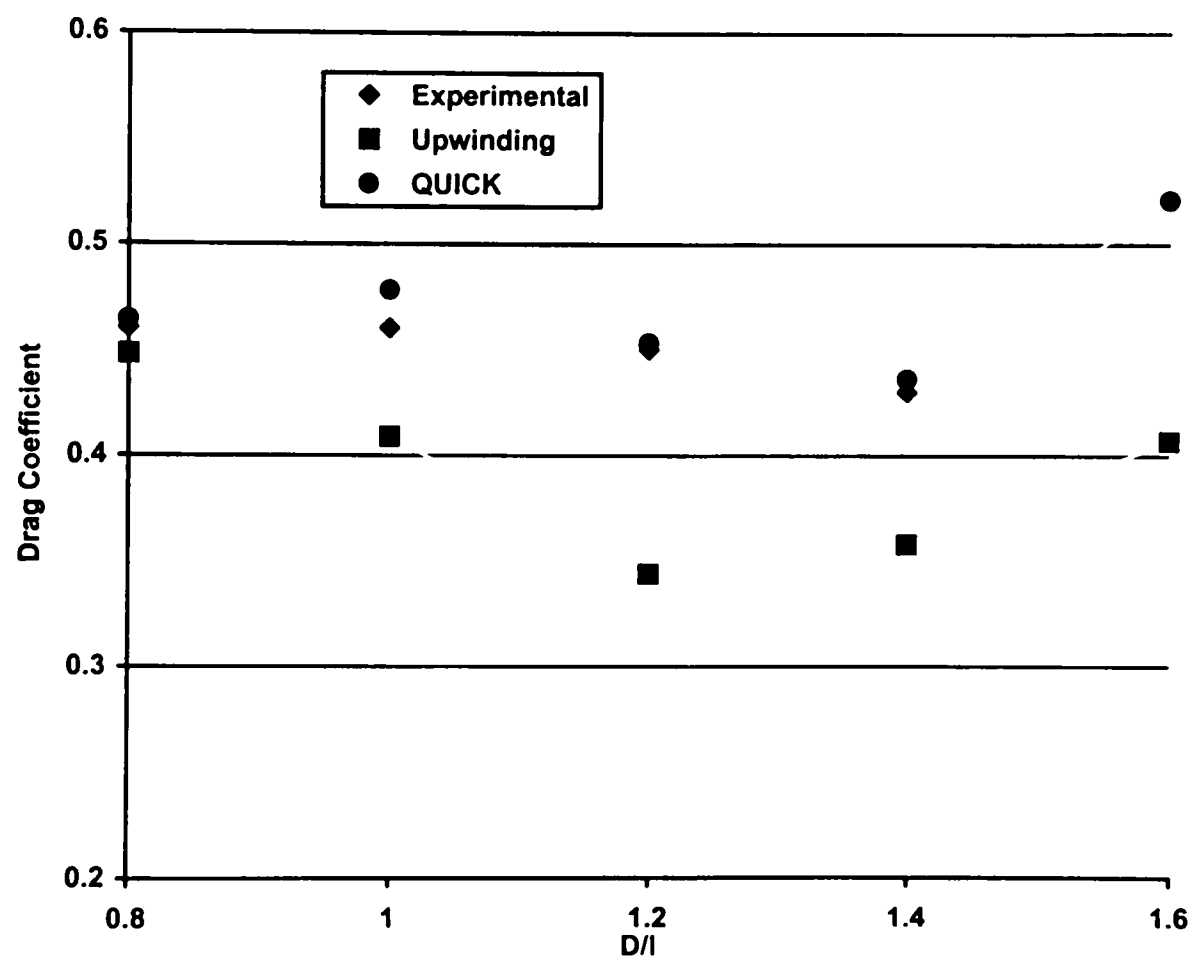
Fig. 7.1 Drag coefficient Versus D/l

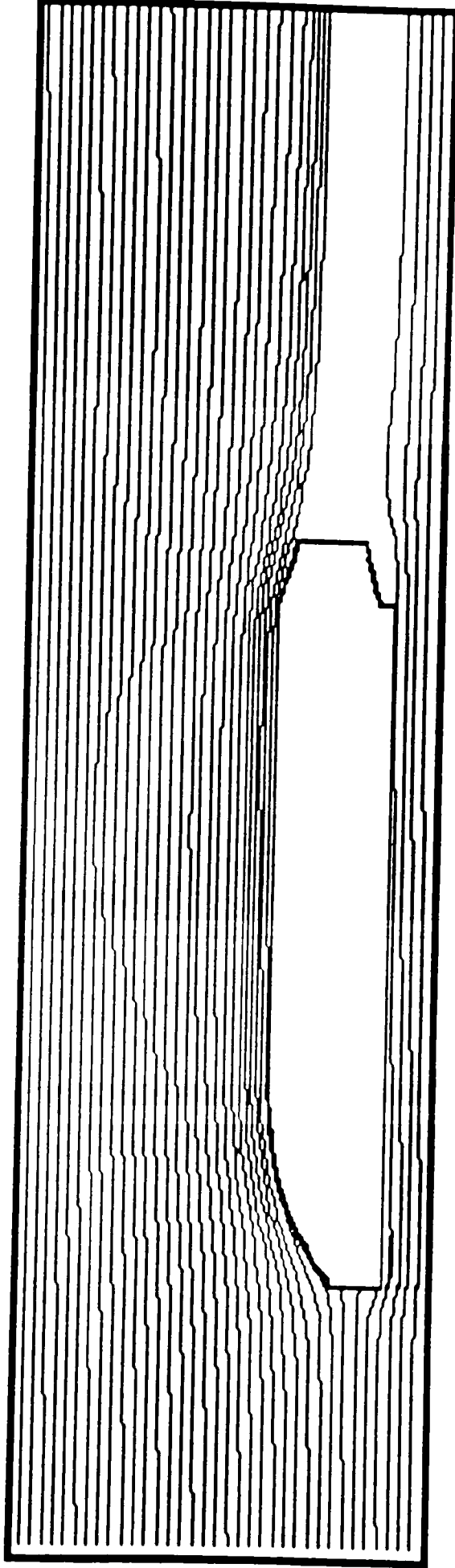Fig. 7.2. Particle traces around a truck without boattail

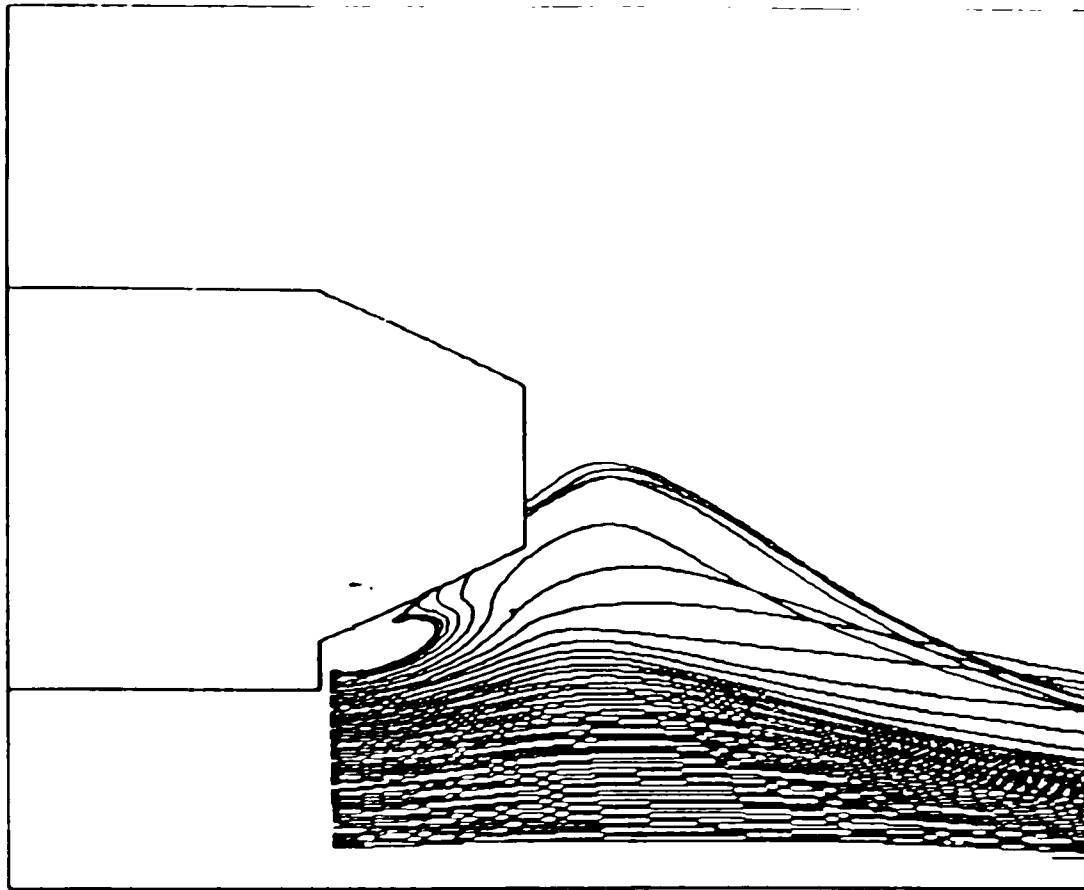Fig. 7.3. Particle traces around a truck with boattail

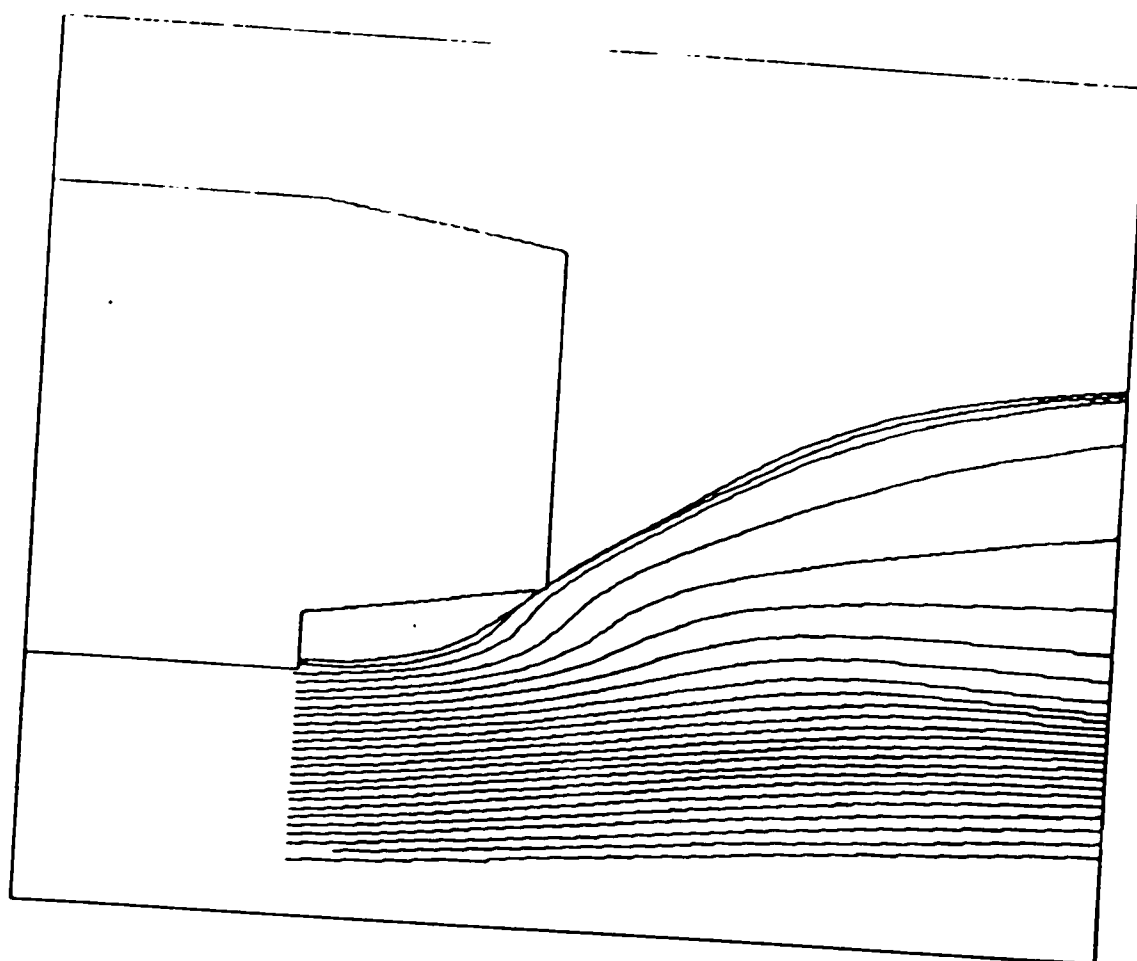Fig. 7.4. Particle trace- enlarged at the rear end for boattail-1

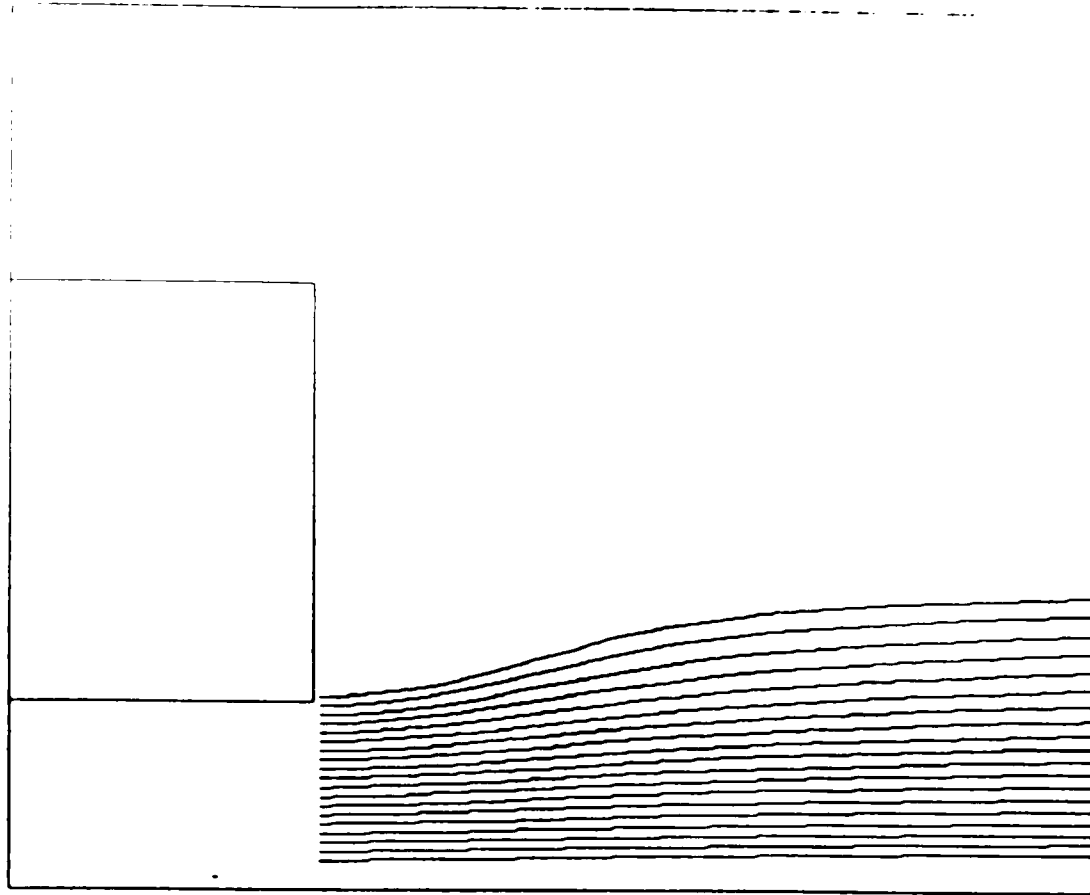Fig. 7.5. Particle traces enlarged at the rear end for boattail-4

Fig. 7.6. Particle traces enlarged at rear around the truck without a boattail
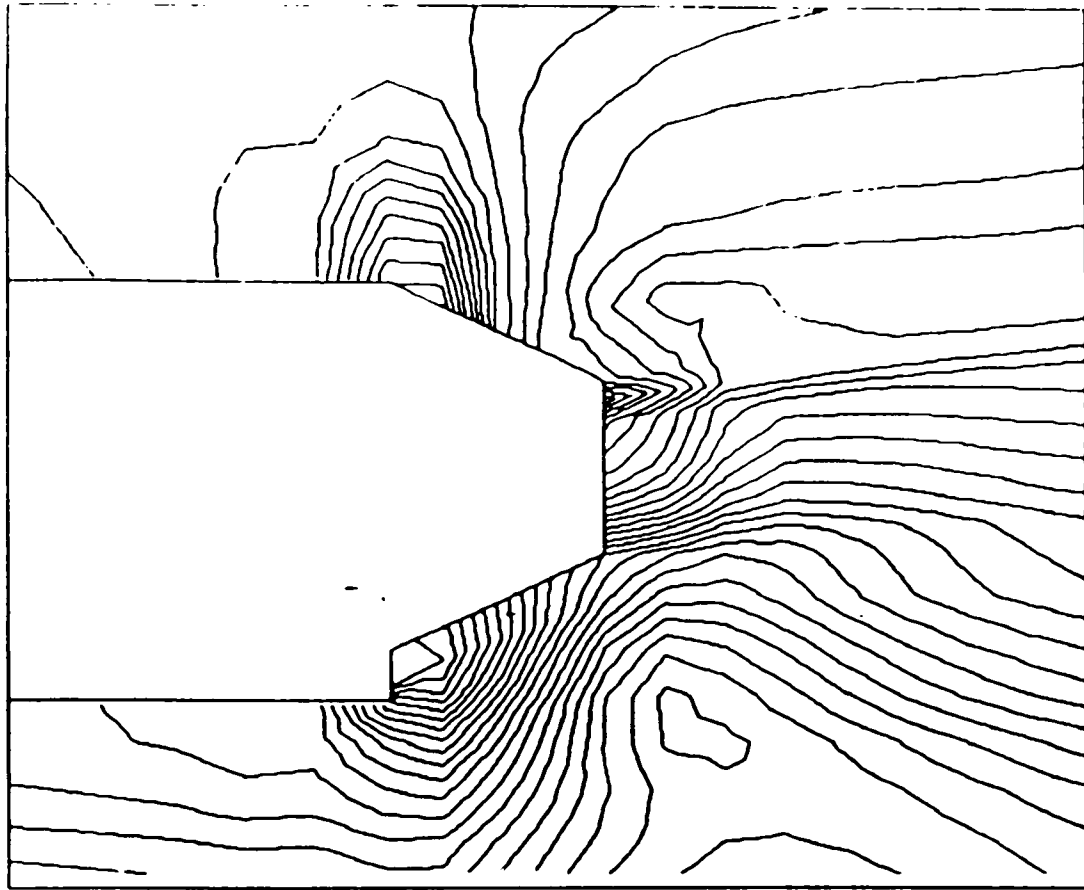
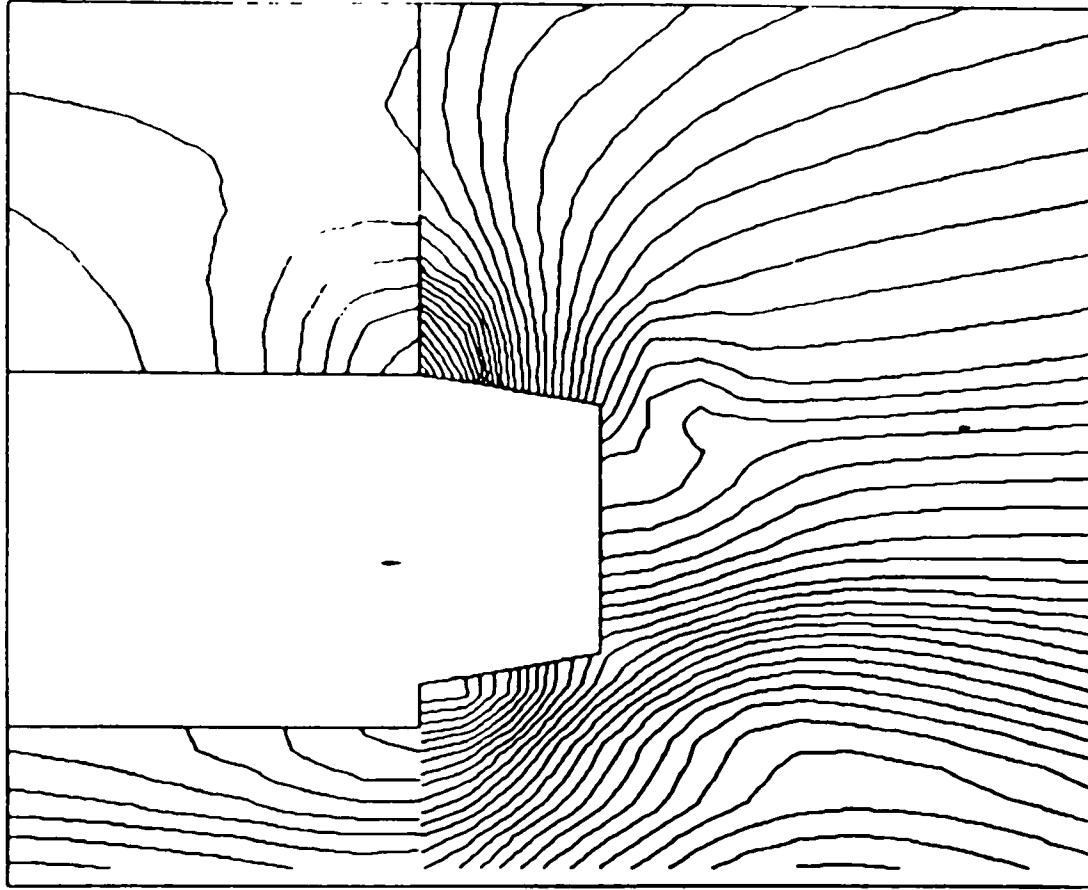Fig. 7.7. Pressure contour - enlarged at the rear end for boattail-1

Fig. 7.8. Pressure contour - enlarged at the rear end for boattail-4

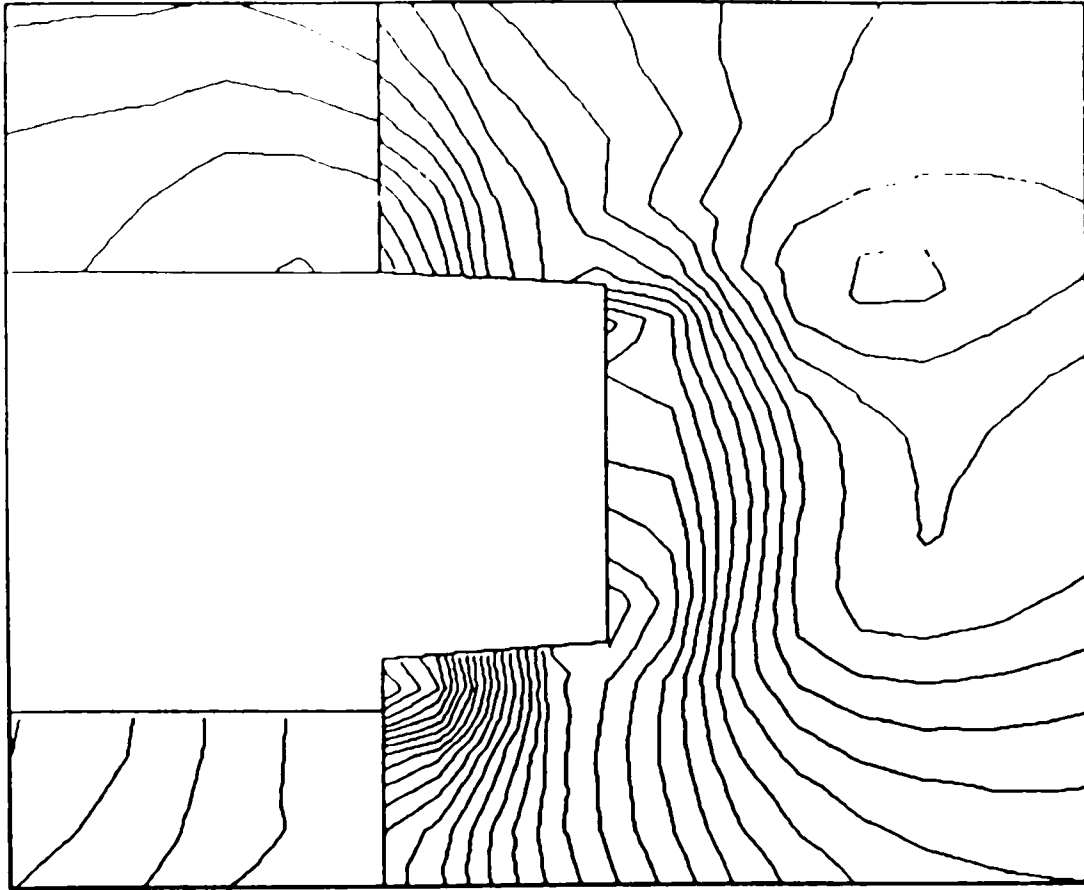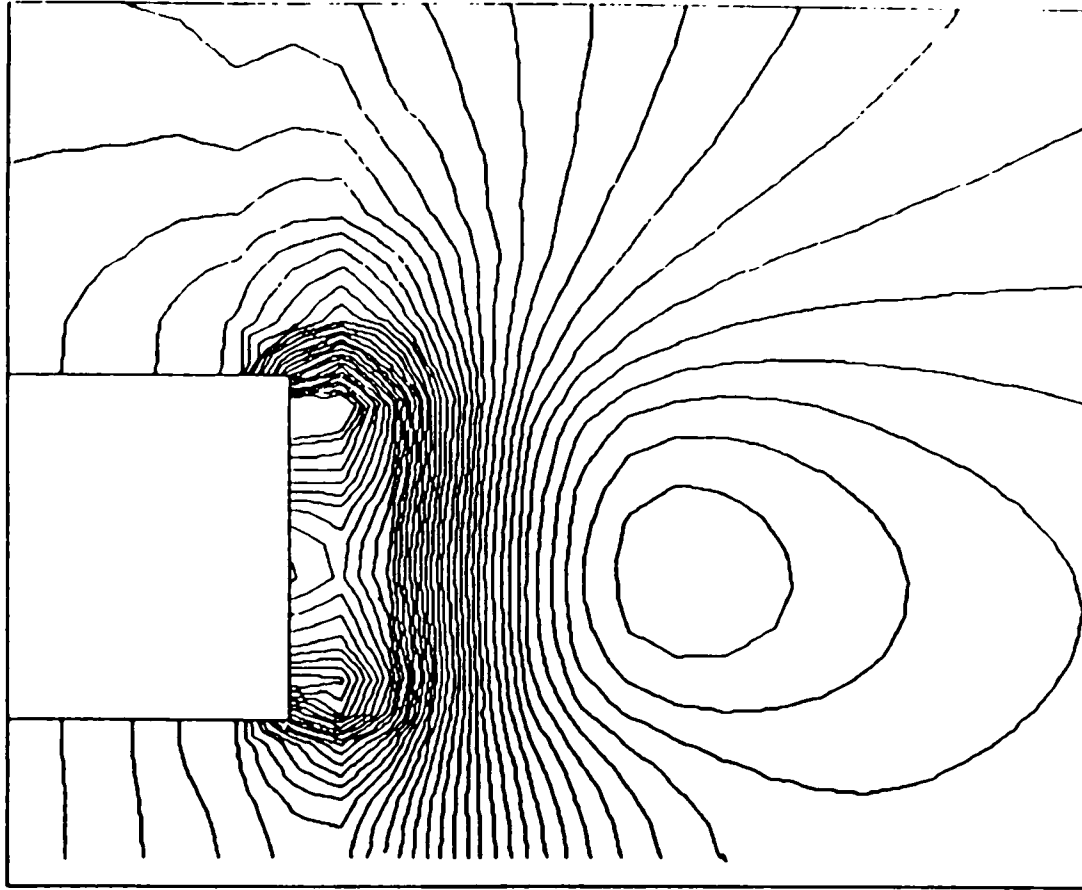Fig. 7.9. Pressure contour enlarged at the rear end for boattail - 5

Fig. 7.10. Pressure contour - enlarged at the rear end for truck without boattail
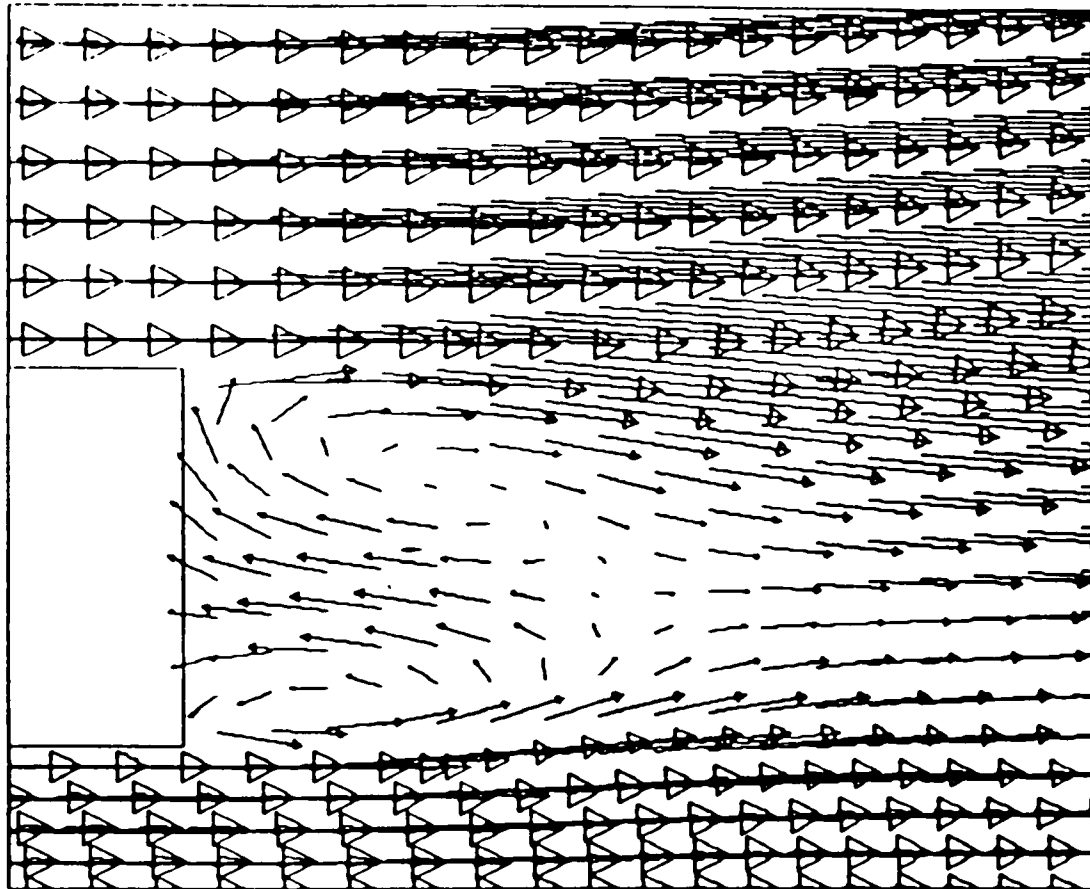
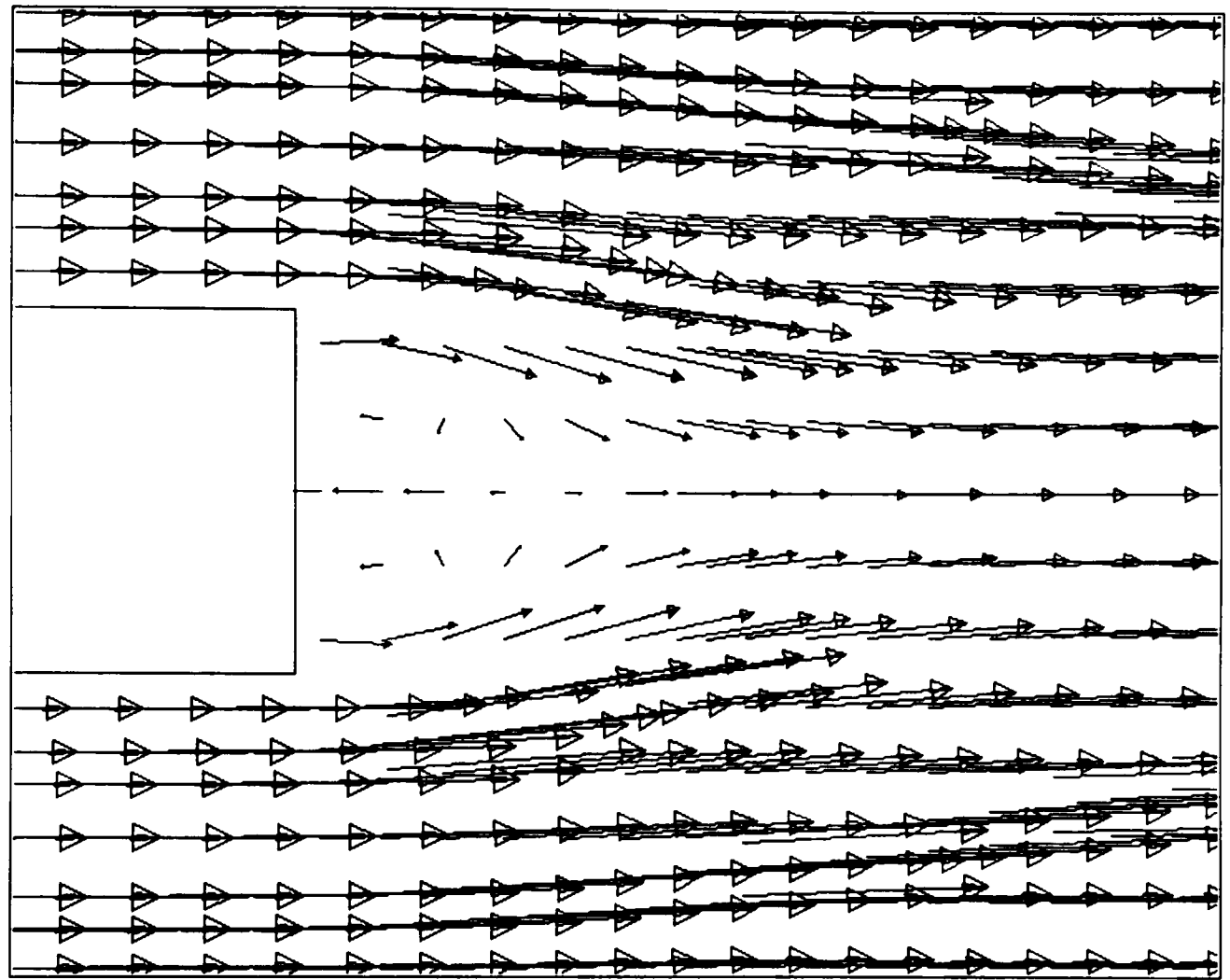Fig. 7.11. Vector arrows around the truck without a boattail - front view

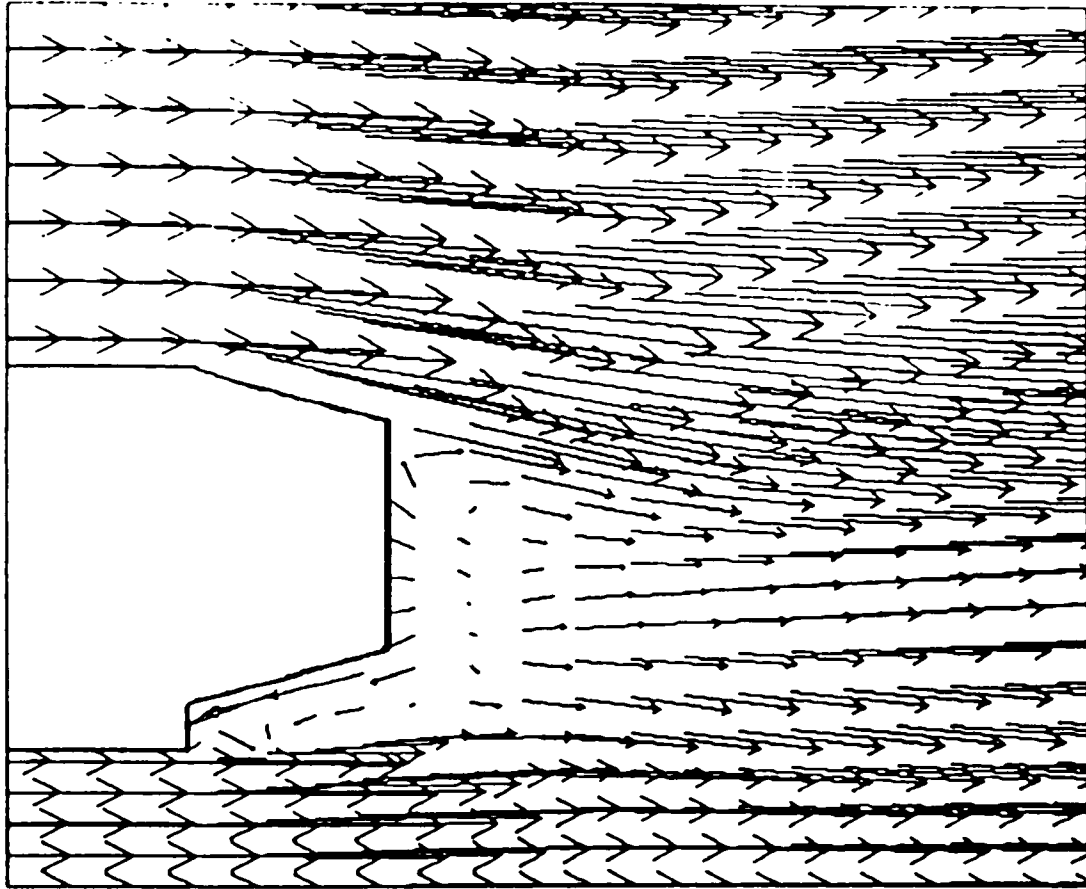Fig. 7.12 Vector arrows for truck without a boattail

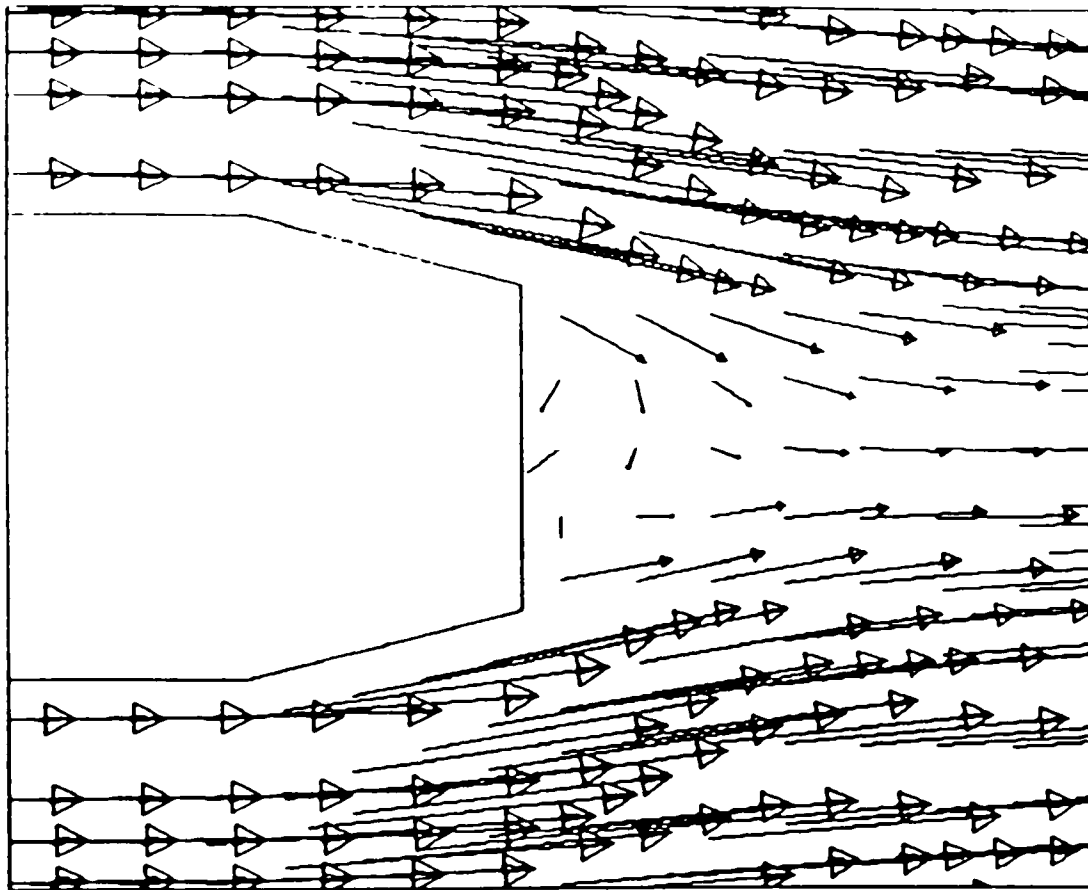Fig. 7.13. Vector arrows truck with a boattail - front view

Fig. 7.14 Vector arrows truck with a boattail -top view

The particle traces shown in Fig. 7.4 and Fig. 7.5 indicate that boattail-1 has a clear case of recirculation beneath the boattail, whereas boattail-4 does not have any recirculation. These patterns justify the trend in drag coefficient. The boattail-5 has almost the same dimension throughout the length of the boattail. This attachment will function as an additional length increment instead of decreasing flow separation. The increase in drag coefficient for boattail-5 can be attributed to the additional skin friction due to the increased length and the low pressure region beneath the boattail.

In the case of truck without a boattail, we see a marked difference in drag coefficient for experimental results and the computational results. Due to the limitation imposed by the software, the number of control volumes in the front and the back of the truck had to be kept equal. Unlike in the case of truck with boattails, we have a wider area in the case of a truck without a boattail which leads to larger control volumes at the rear end. These larger control volumes could have been the cause for the significant amount of discrepancies in drag coefficients between experimental and computational methods.

From the Fig. 7.1, the following conclusions can be made:

- Drag reduction up to 14% can be achieved by the introduction of the boattails to the tractor-trailers.

- The QUICK formulation gives a better results than the upwinding scheme for this type of problems.

- Drag coefficient continues to reduce with the increase in boattail diameter up to boattail-4 and decrease again for boattail-5.

The QUICK formulation has the error of order two ($\Delta x^2$) and the upwinding scheme has an error of order one ($\Delta x$). This is the reason for the better results given by the QUICK formulation

## 7.1. Recommendations for future work

As a continuation of this work, a shape optimization study (a combined use of simulation techniques and an optimization algorithm) can be done to arrive at a better configuration. As suggested by J.S.Brock [1], the direct-iterative inverse design technique would be appropriate for this purpose due to its usability with an existing CFD code. This geometry can be used as the initial geometry in arriving at an optimized shape.

# REFERENCES

1. Brock, J.S.,and Ng, W.F., "Quasi-Analytical Shape Modification for Neighboring    Steady-State Euler Equations," Proceedings of the Period of Concentration in Flow Control, IMA, Nov. 1992.

2. Drollinger, Richard, A., "Heavy Duty Truck Aerodynamics," SAE SP-688, 1987

3. Funderburk, R.S., "An Investigation of a Drag Reducing Device for Tractor-Trailers," Masters Thesis, Texas Tech University, 1996.

4. Han, T., Hammond, D.C., and Sagi, C.J., " Optimization of Bluff Body for Minimum drag in Ground Proximity," AIAA J. Vol. 30, April-1992

5. Hassan, B., Gutierrez, W., Wolfe, W., Walker, M. and Hurt, J., "Numerical Prediction of Aerodynamic Drag for Heavy Ground Transportation Vehicles," AIAA 95-1913, 1995

6. Ilker, K. and Parameswaran, S., "A Multigrid Based Computational Procedure to Predict Internal Flows with Heat Transfer," Proceedings of 30th National Heat Transfer Conference, Vol. 9, 1995

7. Launder, B.P. and Spalding, D.B., Mathematical Models of Turbulence, Academy Press, London, 1972.

8. Leonard, B.P., "A Stable and Accurate Convective Modeling Procedure Based on Quadratic Upstream Interpolation," Computer Models in Applied Mechanics and Engineering, Vol. 19, 1979.

9. Parameswaran, S., Srinivasan, A. and Sun, R., "Numerical Aerodynamics Simulation of Steady and Transient Flows Around Two-dimensional Bluff Bodies Using the Non-Staggered Grid System," Numerical Heat Transfer, Part A, Vol. 21, 1992

10. Patankar, S.V. and Spalding, D.B., "A Calculation Procedure for Heat Mass and Momentum Transfer in Three-Dimensional Parabolic Flows," Int. J. of Heat and Mass Transfer, Vol. 15, 1972.

11. Patankar, S.V., <u>Numerical Heat Transfer and Fluid Flow</u>, Hemisphere, Washington, D.C., 1990

12. Peterson and Randall, L., "Drag Reduction Obtained by the Addition of a Boattail to a Box Shaped Vehicle," NASA Contractor Report 163113, August, 1981

13. Wolf-Heinrich Hucho, Aerodynamics of Road Vehicles, Butterworth-Heinemann, Stoneham, MA, Reprint 1990.

# PERMISSION TO COPY

In presenting this thesis in partial fulfillment of the requirements for a master's degree at Texas Tech University or Texas Tech University Health Sciences Center, I agree that the Library and my major department shall make it freely available for research purposes. Permission to copy this thesis for scholarly purposes may be granted by the Director of the Library or my major professor. It is understood that any copying or publication of this thesis for financial gain shall not be allowed without my further written permission and that any user may be liable for copyright infringement.

**Agree**  (Permission is granted.)

_K. Elakumar_ ,  01/24/97
Student's Signature                                    Date


**Disagree**  (Permission is not granted.)


_____           _____
Student's Signature                                    Date